

Electromagnetic radiation from relativistic nuclear collisions

Charles Gale[†] and Kevin. L. Haglin[§]

[†]*Department of Physics, McGill University
3600 University St., Montréal, QC, H3A 2T8, Canada*

[§]*Department of Physics, Astronomy and Engineering Science
St. Cloud State University, St. Cloud, MN 56301, USA*

We review some of the results obtained in the study of the production of electromagnetic radiation in relativistic nuclear collisions. We concentrate on the emission of real photons and dileptons from the hot and dense strongly interacting phases of the reaction. We consider the contributions from the partonic sector, as well as those from the non-perturbative hadronic sector. We examine the current data, some of the predictions for future measurements, and comment on what has been learnt so far.

Contents

1	Introduction	3
2	Radiation from Hadronic Matter	5
2.1	The Low Dilepton Invariant Mass Sector	7
2.1.1	A Baseline Calculation	7
2.1.2	Spectral Density Calculations	8
2.2	The Dilepton Intermediate Invariant Mass Sector	12
2.3	Photons	24
2.3.1	General Strategy	24
2.3.2	Establishing the Rates	25
2.3.3	Refinements	27
2.3.4	Medium Effects	28
2.3.5	Alternative Approach: Chiral Reduction Formulae	29
3	Radiation from Partons	30
3.1	Photons	30
3.1.1	Photon Measurements	33
3.2	Dileptons	40
4	Predictions	43
4.1	Photons	43
4.2	Dileptons	46
4.3	Electromagnetic Signatures of Jets	48
4.4	Squeezing Lepton Pairs out of Broken Symmetries	54
5	Conclusions	59
	References	61

1. Introduction

The study of matter under extreme conditions constitutes a rich field of intellectual pursuit and is a vibrant research area of physics. It is popularised to nonspecialists by indicating that such studies reveal physics that governed the early Universe (microseconds after the Big Bang) and also continue today to govern physics of compact astrophysical objects (neutron stars and black holes). But it is indeed more than that. Practitioners concern themselves with a variety of very specific and technically challenging questions. When ordinary matter is heated to roughly a trillion degrees Kelvin, how does it respond? And what are the hallmark signatures of this response? What should one look for? When relatively cold matter is compressed to densities many times greater than that of normal nuclei, does it resemble something other than ordinary protons and neutrons? Quantum Chromodynamics (QCD) predicts under these extreme conditions, very far from the ground state, that matter will essentially change its properties to resemble a plasma of quarks and gluons (QGP)^{1,2}. What is the QCD phase diagram?

Indeed, the understanding of QCD under extreme conditions of high temperature or large baryon density has progressed considerably in recent years. Confinement, in the pure glue version of QCD, is a property that can be associated with a definite symmetry whose status is probed by the value of the Polyakov loop $\langle L \rangle$. This symmetry is valid at low temperature, but broken at high temperatures. In the limit of massless quarks, QCD is chirally symmetric, and that symmetry is valid at high temperatures and spontaneously broken at low temperatures. The order parameter there is the chiral condensate: $\langle \bar{\psi}\psi \rangle$. As a function of temperature, those order parameters are best studied on the lattice; although it is fair to say that the lattice has just started to venture into the finite baryon domain with any degree of quantitative assurance³. An idea on the status of finite-temperature lattice QCD can be had by consulting Ref. [1, 2]. The order of the transition actually depends on the details of the parameters of the theory, as shown in the “Columbia plot” (Fig. 1), but even in the absence of a robust prediction at finite temperature and baryon density, the lattice does provide tantalising clues of an eventually observable behaviour of the many-body nature of QCD. For example, it offers some support, together with effective models, to the discussions of a genuine tricritical point in the QCD phase diagram⁴.

The experimental realisation of hot and dense strongly interacting mat-

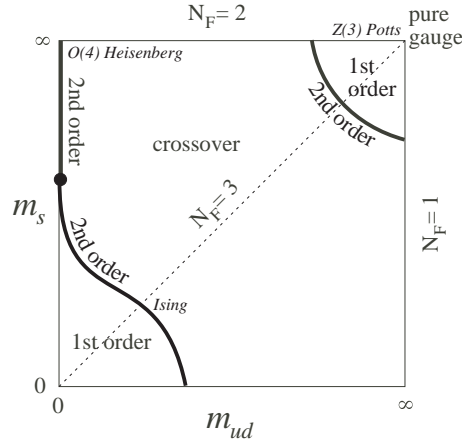


Fig. 1. The nature of the QCD phase transition as a function of quark masses, along with theoretical expectations from effective models. From [2].

ter in terrestrial accelerators has been accomplished through the study of relativistic nuclear collisions. Producing quark gluon plasma (QGP) is one of the premier goals of the Relativistic Heavy Ion Collider (RHIC) and its broader experimental program and represents already enormous challenge; identifying the plasma and also studying its unique properties is yet something else, and has proven to be extremely challenging from both the theoretical and experimental points of view. Signatures of the QGP have been proposed: strangeness enhancement, suppression of the J/ψ signal, effects of multiple collisions on the observed particle spectra, and electromagnetic radiation are but a few. Unfortunately, while most of the proposed signatures are plausible and evidently do occur at some level, it has been difficult to refine the mostly heuristic arguments into really precise predictions. It is now clear that certainty will be attained in this field through the simultaneous analysis of complementary observables. This being said, probes that do not interact strongly have the definite advantage of suffering little or no final state interaction: they open a privileged window to the hot and dense phases of the reaction. The price to pay is a small production rate.

We will discuss in this article the status of theory and the current picture relative to the experimental data, surrounding electromagnetic radiation as probes of strongly-interacting many-body dynamics. This work is organised as follows: a brief review of the formalism germane to the emission of real

and virtual photons from hot and dense systems is followed by a discussion of the radiation from the hadronic sector, then from the partonic sector. Some of predictions for current and future measurements are outlined, followed by a conclusion. The main thrust here pertains to models amenable to conventional experimental measurements: the high density low temperature phase of QCD⁵ will not be discussed, even though its electromagnetic emissivity has been investigated⁶. A goal here is to provide the reader with a snapshot of this rapidly evolving field by discussing some of the recent theoretical and experimental developments. In doing so, it is unfortunately impossible to do justice to the wholeness of the body of work in this exciting area: we shall be brief on some topics and refer instead to the literature and in particular to previous reviews.

2. Radiation from Hadronic Matter

The goal of this section of the text is to relate the spectrum of emitted radiation to some of the intrinsic properties of the strongly interacting matter. A thermalised medium is assumed, and the formalism below is developed in the one-photon approximation.

Quite generally, the electromagnetic radiation from strongly interacting matter can be related to the imaginary part of the retarded in-medium photon self-energy, at finite temperature and density^{7,8,9,10,11}. We sketch a derivation¹¹ here, for the emission of real photons. Consider a transition $i \rightarrow f\gamma$, *i.e.* from some initial hadronic state i to some final hadronic state f , plus a photon of momentum $k^\mu = (\omega, \mathbf{k})$ and polarisation ϵ^μ . The transition rate is

$$R_{fi} = \frac{|S_{fi}|^2}{\tau V}, \quad (1)$$

where τ is the observation time, V is the volume of the system, and the S -matrix element is

$$S_{fi} = \langle f | \int d^4x J_\mu(x) A^\mu(x) | i \rangle. \quad (2)$$

$J_\mu(x)$ is an electromagnetic current operator, and

$$A^\mu(x) = \frac{\epsilon^\mu}{\sqrt{2\omega V}} (e^{ik \cdot x} + e^{-ik \cdot x}). \quad (3)$$

Using translation invariance, summing over polarisations, and using the integral representation of the delta function, one can write

$$R_{fi} = -\frac{g^{\mu\nu}}{2\omega V} (2\pi)^4 [\delta^4(p_i + k - p_f) + \delta^4(p_i - k - p_f)]$$

$$\times \langle f | J_\mu(0) | i \rangle \langle i | J_\nu(0) | f \rangle, \quad (4)$$

where the parts having to do with emission and absorption are evident. The net thermal rate is obtained by summing the above over final states and taking a thermal average of the initial configurations.

It is useful at this point to define some finite-temperature current-current correlators¹²:

$$\begin{aligned} f_{\mu\nu}^>(k) &= \int d^4x e^{ik \cdot x} \sum_i \langle i | A_\mu(x) A_\nu(0) | i \rangle e^{-\beta E_i} / Z, \\ f_{\mu\nu}^<(k) &= \int d^4x e^{ik \cdot x} \sum_i \langle i | A_\mu(0) A_\nu(x) | i \rangle e^{-\beta E_i} / Z, \\ f_{\mu\nu}^R(k) &= \int d^4x e^{ik \cdot x} \sum_i \langle i | [A_\mu(x), A_\nu(0)] | i \rangle e^{-\beta E_i} / Z. \end{aligned} \quad (5)$$

The last correlation function is a retarded correlation function. The above all involve the electromagnetic current operator in the Heisenberg picture and are written in the grand canonical ensemble, where Z is the partition function. Assuming translational invariance, the first two can be rewritten together as

$$f_{\mu\nu}^>(p^0, \vec{p}) = \sum_{i,f} (2\pi)^4 \delta^4(p_f - p_i \pm p) \langle i | A_\mu(0) | f \rangle \langle f | A_\nu(0) | i \rangle e^{-\beta E_i} / Z. \quad (6)$$

Clearly, $f^>$ is involved with absorption of radiation, whereas $f^<$ deals with emission. Only, the latter case is treated here. Further defining a spectral density $\rho_{\mu\nu} = f_{\mu\nu}^> - f_{\mu\nu}^<$, one may first show that

$$f_{\mu\nu}^< = \frac{\rho_{\mu\nu}}{e^{\beta\omega} - 1}, \quad (7)$$

and also that

$$f_{\mu\nu}^R = i \int \frac{d\omega}{2\pi} \frac{\rho_{\mu\nu}(\omega, \vec{k})}{k^0 - \omega + i\epsilon}. \quad (8)$$

With the above elements, one can finally write $\rho_{\mu\nu} = 2 \text{Im} f_{\mu\nu}^R$. The emission probability is related to the imaginary part of the finite-temperature retarded current-current correlation function. In the one-photon approximation (*i.e.* to lowest order in e^2), the time-ordered current correlator is the one-particle irreducible photon self-energy, $\Pi_{\mu\nu}$ ¹³. Putting all of this together, the differential rate for emitting real photons is

$$\omega \frac{d^3 R}{d^3 k} = - \frac{g^{\mu\nu}}{(2\pi)^3} \text{Im} \Pi_{\mu\nu}^R(k) \frac{1}{e^{\beta\omega} - 1}. \quad (9)$$

The proof is easily generalised to the case of lepton pair emission (the lepton mass has been set to zero):

$$E_+ E_- \frac{d^6 R}{d^3 p_+ d^3 p_-} = \frac{2e^2}{(2\pi)^6} \frac{1}{k^4} [p_+^\mu p_-^\nu + p_+^\nu p_-^\mu - g^{\mu\nu} p_+ \cdot p_-] \text{Im}\Pi_{\mu\nu}^R(k) \times \frac{1}{e^{\beta\omega} - 1}. \quad (10)$$

Thus, the electromagnetic signal emitted during a nuclear reactions can be related to a quantity that is linked to properties of the medium itself. As it shall be seen, the retarded self-energy (or alternatively the current-current correlator) will be modified in a strongly interacting environment. Also, the current-current correlator is calculable only perturbatively, unless a specific model is available: this again testifies to the importance and the value of electromagnetic measurement in nuclear collisions. They indeed open a window to the hot and dense phases of the reaction, and those regions can't be probed directly by other means.

2.1. The Low Dilepton Invariant Mass Sector

2.1.1. A Baseline Calculation

As a calculation to set the scale of the physical processes under consideration, it is useful to consider first the following question: what is the magnitude of the radiation emitted by a hot gas of mesons? Specialising to the lepton pair sector¹⁴, this problem is briefly summarised here. Using relativistic kinetic theory, the lepton pair emission rates can be calculated with the help of effective interaction Lagrangians. The parameters of those effective Lagrangians are fitted to radiative decays measurements using vector meson dominance (VMD). Specifically, the “calibration” reactions are: $\rho \rightarrow \pi\gamma$, $K^{*\pm} \rightarrow K^\pm\gamma$, $K^{*0} (\bar{K}^{*0}) \rightarrow K^0 (\bar{K}^0)\gamma$, $\omega \rightarrow \pi^0\gamma$, $\rho^0 \rightarrow \eta\gamma$, $\eta' \rightarrow \rho^0\gamma$, $\eta' \rightarrow \omega\gamma$, $\phi \rightarrow \eta\gamma$, $\phi \rightarrow \eta'\gamma$, and $\phi \rightarrow \pi^0\gamma$. Note that the usage of relativistic kinetic theory here is tantamount to evaluating the finite temperature photon self-energy at the one-loop level¹¹. The rate for $ab \rightarrow e^+e^-$ is given by

$$R_{ab \rightarrow e^+e^-} = \mathcal{N} \int \frac{d^3 p_a}{2E_a (2\pi)^3} \frac{d^3 p_b}{2E_b (2\pi)^3} \frac{d^3 p_+}{2E_+ (2\pi)^3} \frac{d^3 p_-}{2E_- (2\pi)^3} f_a f_b \times |\bar{\mathcal{M}}|^2 (2\pi)^4 \delta^4(p_a + p_b - p_+ - p_-), \quad (11)$$

where the f 's are appropriate distribution functions, and \mathcal{N} is an overall degeneracy factor dependent upon the specific channel. The $PP \rightarrow e^+e^-$,

$PV \rightarrow e^+e^-$, and $VV \rightarrow e^+e^-$ reactions can be obtained from the radiative decay ones through crossing symmetry. The sum of them is shown in Fig. 2. Also shown is the contribution from the $\pi^+\pi^- \rightarrow e^+e^-$ reaction. This channel has often been considered as the sole source of hadronic dileptons in early calculations, owing mainly to multiplicity arguments. Even in this incoherent sum approach, one can see that this assumption is badly violated in the low mass region.

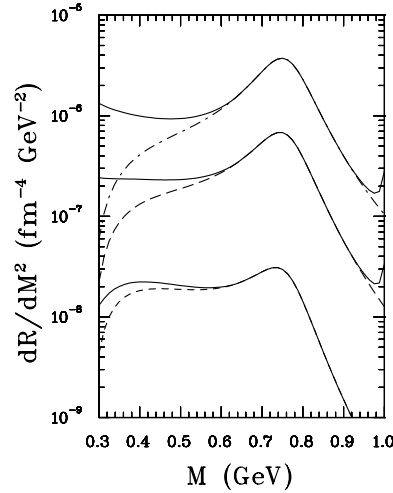


Fig. 2. The rates for dielectron emission from an incoherent sum of meson reactions¹⁴. The three sets of full curves are the net rates at a temperature of 100, 150, and 200 MeV, from bottom to top. The dashed curves represent the $\pi^+\pi^- \rightarrow e^+e^-$ contribution only.

2.1.2. Spectral Density Calculations

The full power of the formalism derived in section 2 reveals itself when it is made clear that the electromagnetic radiation rate is related to the in-medium vector meson spectral density: this quantity is of course not measurable directly. The spectral density is related to the imaginary part of the full propagator, by definition. It appears when the electromagnetic current operator in the retarded self-energy is expressed as the field operator, through VMD^{18,19,20}. We illustrate the spectral density approach here, by describing a calculation again done in the baryonless regime²¹.

One may start with the model for the ρ -meson in free space employed

previously in Refs. [15, 16, 17]. Based on the standard $\rho\pi\pi$ interaction vertex (isospin structure suppressed),

$$\mathcal{L}_{\rho\pi\pi} = g_{\rho\pi\pi} \pi p^\mu \pi \rho_\mu, \quad (12)$$

(p^μ : pion momentum) the bare ρ -meson of mass m_ρ^0 is renormalised through the two-pion loop including a once-subtracted dispersion relation, giving rise to the vacuum self-energy

$$\begin{aligned} \Sigma_{\rho\pi\pi}^0(M) &= \bar{\Sigma}_{\rho\pi\pi}^0(M) - \bar{\Sigma}_{\rho\pi\pi}^0(0), \\ \bar{\Sigma}_{\rho\pi\pi}^0(M) &= \int \frac{p^2 dp}{(2\pi)^2} v_{\rho\pi\pi}(p)^2 G_{\pi\pi}^0(M, p), \end{aligned} \quad (13)$$

with the vacuum two-pion propagator

$$G_{\pi\pi}^0(M, p) = \frac{1}{\omega_\pi(p)} \frac{1}{M^2 - (2\omega_\pi(p))^2 + i\eta}; \quad \omega_\pi(p) = \sqrt{m_\pi^2 + p^2}, \quad (14)$$

and vertex functions

$$v_{\rho\pi\pi}(p) = \sqrt{\frac{2}{3}} g_{\rho\pi\pi} 2p F_{\rho\pi\pi}(p), \quad (15)$$

involving a hadronic (dipole) form factor $F_{\rho\pi\pi}$ ¹⁷. Resumming the two-pion loops in a Dyson equation gives the free ρ propagator

$$D_\rho^0(M) = [M^2 - (m_\rho^0)^2 - \Sigma_{\rho\pi\pi}^0(M)]^{-1}, \quad (16)$$

which agrees well with the measured p -wave $\pi\pi$ phase shifts and the pion electromagnetic form factor obtained within VMD.

To calculate medium corrections to the ρ self-energy in a hot meson gas, one can assume that the interactions are dominated by s -channel resonance formation. It is then possible to use the formal relationship that relates the self-energy to the forward scattering amplitude, integrated over phase space at finite temperature. A field-theoretic derivation of this connection can be found in [22]. At moderate temperatures relevant for the hadronic gas phase, the light pseudoscalar Goldstone bosons $P = \pi, K$ are the most abundant species. The various resonances in ρP collisions can be grouped into two major categories, namely vector mesons V and axial-vector mesons A . The effective Lagrangians that regulate the interactions among all those species have their parameters chosen such that the measured hadronic phenomenology are reproduced²¹. This statement also holds true for hadronic form factors. In order to calculate the ρ spectral density at moderate temperatures, one includes the hadronic fields appearing in Table 1. The interaction vertices being completely determined, one may

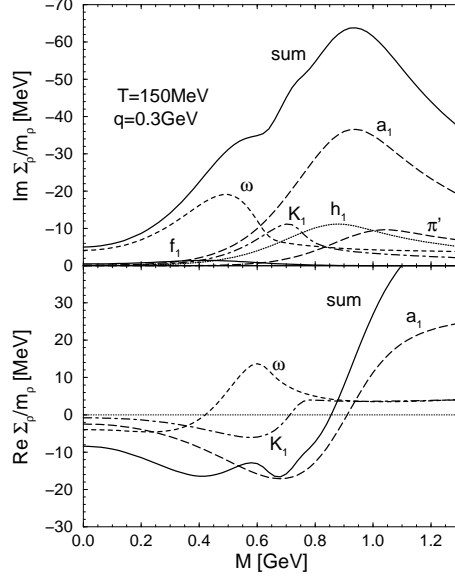


Fig. 3. The real and imaginary parts of the polarisation-averaged ρ self-energy (lower and upper panel, respectively). The different channels are labelled explicitly and are explained in the text²¹. Note that the $\pi\pi$ channel is absent for the sake of viewing clarity.

Table 1. Mesonic resonances R with masses $m_R \leq 1300$ MeV and substantial branching ratios into final states involving direct ρ 's (hadronic) or ρ -like photons (radiative). Taken from Ref. [21].

R	$I^G J^P$	Γ_{tot} [MeV]	ρh Decay	$\Gamma_{\rho h}^0$ [MeV]	$\Gamma_{\gamma h}^0$ [MeV]
$\omega(782)$	$0^- 1^-$	8.43	$\rho\pi$	~ 5	0.72
$h_1(1170)$	$0^- 1^+$	~ 360	$\rho\pi$	seen	?
$a_1(1260)$	$1^- 1^+$	~ 400	$\rho\pi$	dominant	0.64
$K_1(1270)$	$\frac{1}{2} 1^+$	~ 90	ρK	~ 60	?
$f_1(1285)$	$0^+ 1^+$	25	$\rho\rho$	≤ 8	1.65
$\pi'(1300)$	$1^- 0^-$	~ 400	$\rho\pi$	seen	?

first calculate the in-medium ρ self-energy, then the complete propagator in terms of its longitudinal and transverse parts¹¹. The real and imaginary parts of the in-medium ρ self-energy are shown in Fig. 3. Each curve is labelled according to that species which interacts with the ρ . It is instructive to observe that the imaginary parts all add, while there is a significant amount of cancellation of the real parts. The first effect creates a sizeable

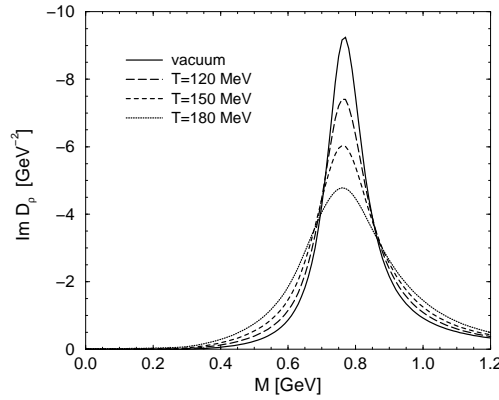


Fig. 4. Imaginary part of the ρ propagator in the vacuum (solid curve) and in a thermal gas including the full in-medium self-energies for fixed three-momentum $q = 0.3$ GeV at temperatures $T = 120$ MeV (long-dashed curve), $T = 150$ MeV (dashed curve), and $T = 180$ MeV (dotted curve). The figure comes from Ref. [21].

width for the in-medium ρ , while the second determines the in-medium mass, which appears to be only slightly modified. Those different aspects are again seen in the representation of the imaginary part of the in-medium ρ propagator, shown in Fig. 4.

The calculations of the in-medium vector meson spectral densities clearly show the richness of the many-body problem under scrutiny. The power of the techniques described above becomes evident when they are combined with dynamical models and confronted with experimental data. This story is well chronicled in [23, 24], and in references therein. See also [25]. The current situation can be summarised by writing that the low dilepton invariant mass data^{26,27} can be understood in terms of in-medium modifications of vector spectral densities. These data can not empirically exclude, however, other interpretations^{28,23,29}. This unfortunate situation still prevails at a lower energy³⁰, as shown in Fig. 5. The sources there are: free hadron decays without ρ decay (thin solid line), calculation with a vacuum ρ spectral density (thick dashed line), dropping in-medium ρ mass²⁸ (dash-dotted line), and with a medium-modified ρ spectral density²⁴ (thick solid line). Note that but the persistence of the dilepton excess at lower energies does support a baryon density-driven effect. Other suggestions to resolve the different models require high statistics²³: the final analysis of

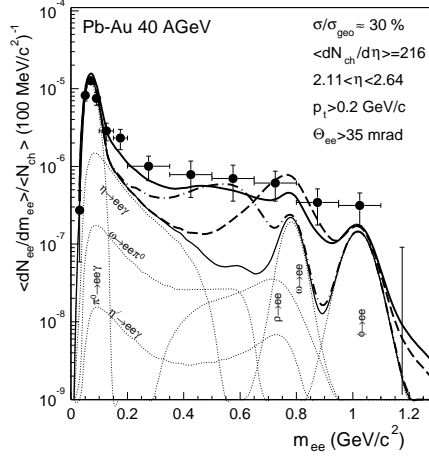


Fig. 5. Dilepton spectrum from Pb-Au collisions at 40 AGeV/c. See the text for the meaning of the different curves. Data are from [30].

the CERES 2000 data with the TPC is eagerly anticipated.

2.2. The Dilepton Intermediate Invariant Mass Sector

Intermediate mass lepton pairs have traditionally been a focus of interest, as their spectrum has been suggested early on as a signature of the quark-gluon plasma³¹. In relativistic nuclear collisions, measurements have been carried out at SPS energies by the HELIOS-3 and the NA38/NA50 collaborations in the lepton pair invariant mass range $m_\phi < M < m_{J/\psi}$. Both experimental collaborations have observed significant enhancement of dilepton yield in this region for central S + W and S + U collisions as compared to those in proton-induced reactions (normalised to the charged-particle multiplicity)^{32,33}. Chronologically, HELIOS-3 reported on the intermediate-mass enhancement first. This experiment was designed to study virtual photons in the dimuon sector at low transverse mass. In this way, dimuon production was studied from threshold up the J/ψ mass over a wide range in p_T . A good summary of this experimental situation is shown in Fig. 6. Several explanations of the intermediate mass dimuon enhancement have been put forward. Those include additional production of $c\bar{c}$ pairs³⁴, secondary Drell-Yan emission³⁵, and charmed meson rescattering³⁶. Note that in principle, all of those effects can coexist. However, such a global modelling has not been done, and we thus discuss them separately. It is

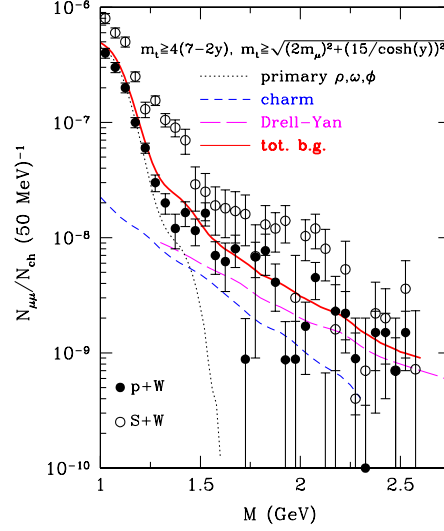


Fig. 6. Comparison of lepton-pair yield divided by the multiplicity of charged particles, in $p + W$ and $S + W$ collisions at 200 A GeV/c. The data are from [27].

fair to say that the first of those mentioned above is still admitted by current experimental data³⁷, even though some calculations are slightly less optimistic³⁸. The role of the last ingredient on the list has not been found to be large enough to account for the experimentally observed excess^{39,37}.

Another class of approaches consists of quantitative evaluation of thermal dilepton sources. Those may be from the hadronic, confined sector of QCD, and/or from the quark gluon plasma itself. One such model is described below. Recall that thermal hadronic sources have been shown to be crucial in the low mass sector. It is therefore legitimate to ask how high in invariant mass is the extent of the virtual photon radiation from those sources? Those concerns are carried to their logical conclusion in what follows.

In the intermediate invariant mass region, relativistic theory estimates indicate that the following microscopic channels are relevant: $\pi\pi \rightarrow l^+l^-$, $\pi\rho \rightarrow l^+l^-$, $\pi\omega \rightarrow l^+l^-$, $\pi a_1 \rightarrow l^+l^-$, $K\bar{K} \rightarrow l^+l^-$, and $K\bar{K}^* + c.c. \rightarrow l^+l^-$ [40]. Apart from sheer coupling constant values, the importance of those contributions stems simply from considering energy scales involved and

from phase space arguments. This combination of coupling constants and phase space is effective in maximising a particular contribution from the πa_1 channel, for example⁴¹.

Calculations of dilepton-emitting processes in the intermediate invariant mass region follow similar steps to those in the low mass sector. Effective Lagrangians are used, together with VMD, and the coupling constants and possible form factors are fitted to measured strong decays and electromagnetic radiative decays. Only, in the intermediate mass domain an extrapolation is required. The strong decay widths set a scale that is typically an order of magnitude below the mass region of interest: $1 \text{ GeV} < M < 3 \text{ GeV}$. The radiative decays are even smaller, owing to the size of α_{em} [42]. The required extrapolation is then vulnerable to off-shell effects. Put another way, there is a risk of uncontrolled growth of form factors since the application region is far removed from the region where the empirical fitting was realized. Indeed, different Lagrangians known to agree in the low mass sector generating dileptons were found to differ significantly in their predictions of emission rates for intermediate mass lepton pairs⁴³. Fortunately, there exists a wealth of data for $e^+e^- \rightarrow \text{hadrons}$, exactly in the invariant mass window relevant for this application. Those data can thus be used to extract an effective form factor for the inverse reactions. Alternatively, they may also be used to extract spectral densities: this point will be discussed later. As an example, consider $e^+e^- \rightarrow \pi^+\pi^-$, which has been measured with high accuracy^{44,45}, evidenced by the data shown in Fig. 7. The cross section for this reaction can be written as

$$\sigma(e^+e^- \rightarrow \pi^+\pi^-) = \frac{8\pi\alpha^2 k^3}{3M^5} |F_\pi(M)|^2, \quad (17)$$

where k is the three-momentum in the two-body rest frame, M is the lepton-pair invariant mass, and F_π is the time-like pion electromagnetic form factor. With these data, one can extract F_π , and then use it in the calculation of the dilepton-producing reaction $\pi^+\pi^- \rightarrow l^+l^-$:

$$\sigma(\pi^+\pi^- \rightarrow l^+l^-) = \frac{8\pi\alpha^2 k}{3M^3} |F_\pi(M)|^2 \left(1 - \frac{m_l^2}{M^2}\right) \left(1 + \frac{2m_l^2}{M^2}\right), \quad (18)$$

where m_l is the lepton mass. A similar procedure can be followed for other channels. Another example appears in Fig. 8, where the time-like electromagnetic form factors for the kaon systems have been extracted from electron-positron annihilation data. Both processes introduced above are of the pseudoscalar-pseudoscalar type. For the pseudoscalar-vector class, in the invariant mass region of interest, $\pi\rho \rightarrow l^+l^-$, $\bar{K}K^* + \text{c.c.} \rightarrow l^+l^-$, and

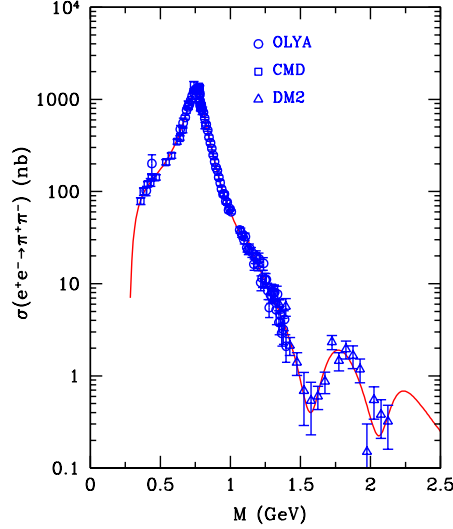


Fig. 7. The cross section for $e^+e^- \rightarrow \pi^+\pi^-$. The solid curve is based on the model of Ref. [46]. The experimental data are from the OLYA collaboration⁴⁴, the CMD collaboration⁴⁴, and the DM2 collaboration⁴⁵.

$\pi\omega \rightarrow l^+l^-$ are included. The first two processes effectively involve three pions, while the third one involves four pions. Note that in a transport approach, a process involving three or more pions in the initial state can only be described as a two-step process with an intermediate resonance. The first two channels above have been studied in Ref. [50]. The effective form factors one extracts are shown in [40]. Details about the $\pi\omega$ channel are gotten from the study of four-pion final states. Using a Wess-Zumino VVP interaction Lagrangian, one finds

$$\sigma(\pi^0\omega \rightarrow l^+l^-) = \frac{4\pi\alpha^2k}{9M} |F_{\pi\omega}(M)|^2, \quad (19)$$

in the limit of vanishing lepton mass. The form factor may be parametrised in terms of three isovector ρ -like vector mesons, $\rho(770)$, $\rho(1450)$, and $\rho(1700)$ ⁵¹:

$$F_{\pi\omega}(M) = \sum_V g_{V\pi\omega} \frac{e^{i\phi_V} m_V^2}{(m_V^2 - M^2) - im_V \Gamma_V}. \quad (20)$$

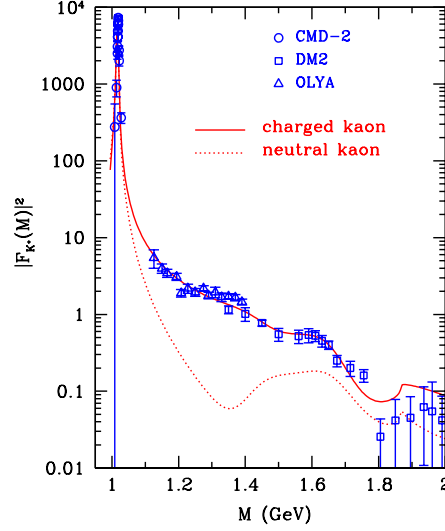


Fig. 8. The kaon electromagnetic form factor. The solid and dotted curves⁴⁶ are for the charged and neutral kaons, respectively. The symbols are for the charged kaon data from the CMD-2 collaboration⁴⁷, the DM2 collaboration⁴⁸, and the OLYA collaboration⁴⁹.

This form is then used to fit the experimental data from the ND and ARGUS collaborations. The result is shown in Fig. 9.

In the pseudoscalar axial-vector channel, we shall consider mainly $\pi a_1 \rightarrow l^+ l^-$, which is in effect a four-pion process. Considering here again the reaction where the lepton pair constitutes the initial state and the hadrons the final, one can attempt an extraction of an effective form factor. Some previous thermal rate calculations indicate that this specific channel is particularly important in the intermediate mass region⁴¹, even though it is difficult to calculate reliably a specific signal using effective Lagrangians. This fact owes mainly to off-shell effects⁴³. One can pick a model that yields adequate hadronic phenomenology on-shell, and then extrapolate to the intermediate mass sector with the help of experimental data. Using a chiral Lagrangian where the vector mesons are introduced as massive Yang-Mills fields⁵³ one may derive the following cross section

$$\sigma(\pi a_1 \rightarrow l \bar{l}) = \frac{\pi \alpha \mathcal{H}}{72 m_{a_1}^2 g_\rho^2 M^5 k_\pi} |F_{\pi a_1}|^2 \left(1 - \frac{4m_l^2}{M^2}\right) \left(1 + \frac{2m_l^2}{M^2}\right), \quad (21)$$

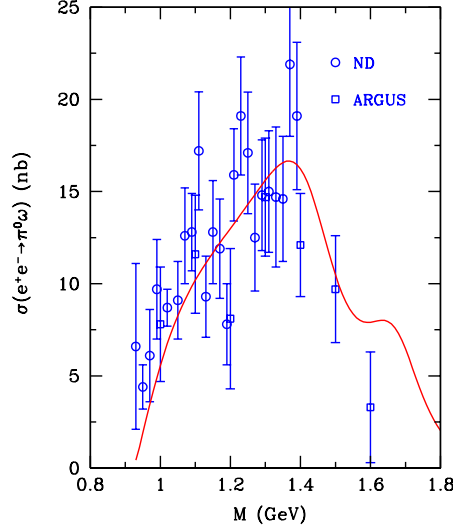


Fig. 9. The cross section for $e^+e^- \rightarrow \pi^0\omega$. The solid curve is described in the text. The experimental data are from the ND⁵¹ and ARGUS⁵² collaborations.

where \mathcal{H} is a nontrivial function of coupling constants, masses and momenta. k_π is the magnitude of the pion momentum in the centre-of-mass. The issue of the electromagnetic form factor $|F_{\pi a_1}|^2$, can be settled, at least in principle, by analysing $e^+e^- \rightarrow \pi^+\pi^-\pi^+\pi^-$ and $e^+e^- \rightarrow \pi^+\pi^-\pi^0\pi^0$ data. Although many such analyses have been carried out, an unambiguous result is still elusive, as many other intermediate states may contribute to the same four-pion final state. Several scenarios have been considered, and a discussion appears in [40]. What is probably a conservative estimate is highlighted here. The DM2 collaboration has determined the cross section $\sigma_{e^+e^- \rightarrow \pi a_1}$ using a partial wave analysis (PWA)⁵⁴. One may extract an effective form factor from these data, see Fig. 10, and then carry out an analysis for $\sigma_{\pi a_1 \rightarrow l\bar{l}}$, using detailed balance.

Even in a careful analysis of the relevant intermediate invariant mass dilepton reactions, some concerns remain. These mainly stem from the need to account for all the sources of electromagnetic radiation. In kinetic theory approaches, risks exist of double-counting and possible omissions. In an attempt to bypass those, an approach which allows for a nonperturba-

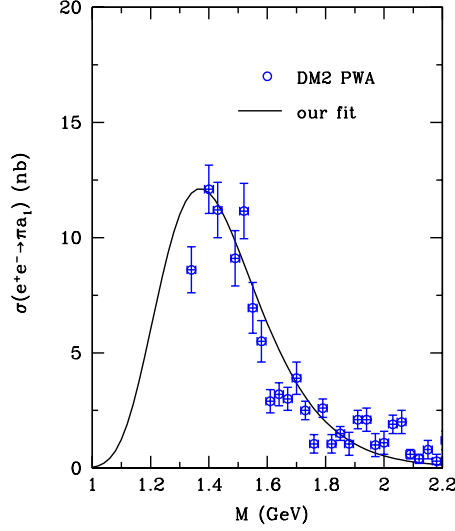


Fig. 10. The cross section for $e^+e^- \rightarrow \pi a_1$. The open circles are the experimental data from the DM2 collaboration using a partial wave analysis⁵⁴. The solid curve is a fit to the data.

tive treatment of the strong interaction and avoids a detailed enumeration of reactions was devised⁵⁵. The dilepton emission rate is interpreted in terms of spectral functions of hadronic currents, tabulated from low energy e^+e^- annihilation reactions and from τ lepton decays. A differential rate expression, obtained in the chiral ($m_\pi \rightarrow 0$) limit, reads⁵⁵

$$\frac{dR}{dM^2} = \frac{4\alpha^2}{2\pi} M T K_1(M/T) \times \left[\rho^{em}(M) - \left(\epsilon - \frac{\epsilon^2}{2} \right) (\rho^V(M) - \rho^A(M)) \right], \quad (22)$$

where T is the temperature, $\epsilon = T^2/6F_\pi^2$, M is the dilepton invariant mass, and the superscripts on ρ denote the electromagnetic, vector, and axial spectral functions, respectively. These spectral distributions are displayed in Fig. 11. Using the spectral functions to generate the lepton pair emission rate, a comparison with the rates obtained via a summation of mesonic reaction channels is shown in Fig. 12. To summarise, the contributing channels producing lepton pairs in the invariant mass range $1 \text{ GeV} < M < 3$

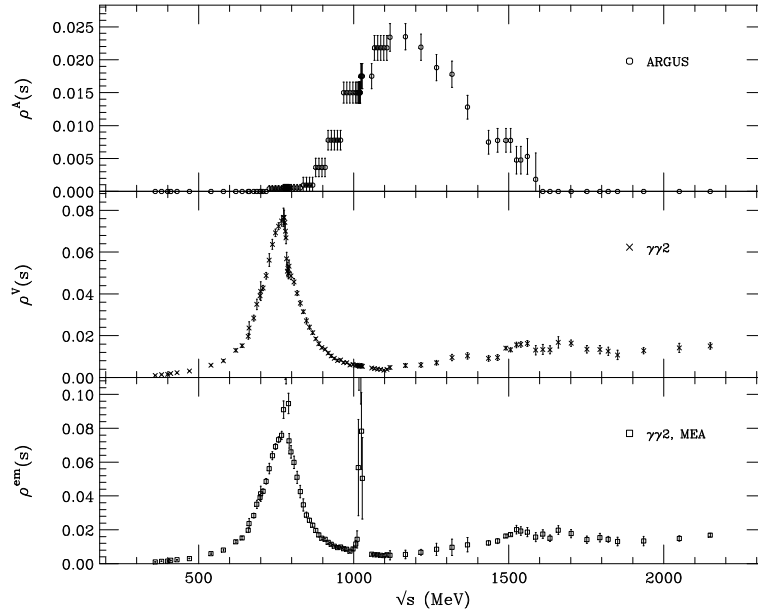


Fig. 11. The spectral functions $\rho^{em}(s)$, $\rho^V(s)$, and $\rho^A(s)$, as compiled from e^+e^- annihilation and τ decay data⁵⁵.

GeV have been found to correspond to the initial states $\pi\pi$, $\pi\rho$, $\pi\omega$, $\eta\rho$, $\rho\rho$, πa_1 , $K\bar{K}$, $K\bar{K}^* + \text{c.c.}$ [56]. The detailed channel-by-channel assessment clearly accounts for the net signal yielded by the “global” spectral function analysis.

In order to compare with experimental data, the rates must be time-integrated in a model that is also compatible with other measured observables, hadronic or otherwise. Furthermore, a precise simulation of the detector acceptance and resolution is necessary. An approach that incorporates both aspects is described presently. A class of models that produce time-evolution scenarios is that of hydrodynamic models. Specifically, the assumption is that, at SPS energies, a plasma is produced at proper time τ_0 . Assuming isentropic expansion, the temperature and proper formation time can be related to the measured differential multiplicity⁵⁸

$$\frac{2\pi^4}{45\zeta(3)} \frac{1}{A_T} \frac{dN}{dy} = 4aT_0^3\tau_0. \quad (23)$$

dN/dy is the measured particle rapidity density and $a = 42.25\pi^2/90$ for a plasma of massless u , d , s , g partons. Once the transverse area A_T is known

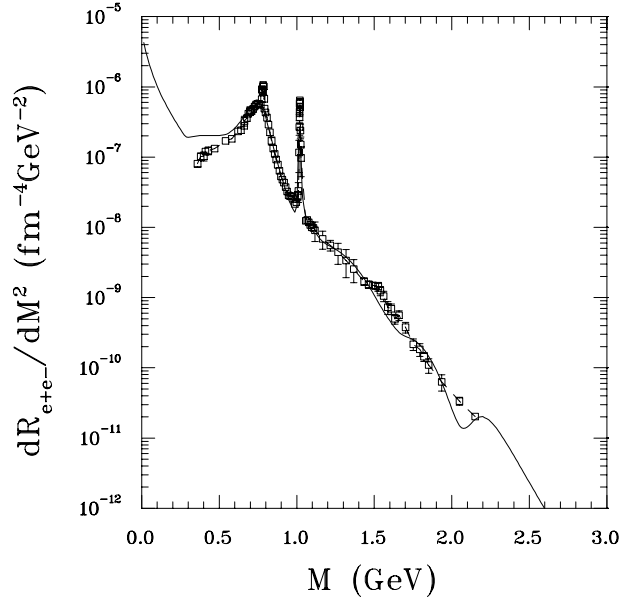


Fig. 12. Net dilepton production from a gas of mesons at a temperature of $T = 150$ MeV, as a function of dilepton invariant mass. The solid curve is the sum of the hadronic channels discussed in the text and in the references. The data points are from [57].

along with dN/dy , the above relation links T_0 with τ_0 . Enumeration of the model premises is completed by the statement that the plasma is assumed to undergo a boost-invariant longitudinal expansion and an azimuthally-symmetric radial expansion, with a transition to a hot hadronic gas consisting of *all* hadrons having $M < 2.5$ GeV, in thermal and chemical equilibrium at temperature T_c . This makes for a rich equation of state. Once all parton matter is converted into hadronic matter, expansion continues until a kinetic freeze-out temperature T_F is reached. Those steps are generic in hydrodynamic calculations. Note that during the evolution, the speed of sound in matter is consistently calculated at every temperature that is input into the equation of state and needed to solve the hydrodynamic equations⁵⁹. Additional details about setting up the initial conditions for the hydrodynamic evolution can be found in Ref. [60]. The same reference also shows the result of hadronic spectra calculations with the hydrodynamic approach.

It is vital to account for the finite acceptance of the detectors and for their resolution when comparing the results of theoretical calculations with

measured experimental data. In the case at hand, those effects are indeed important in the NA50 experiment³⁷. One approach to this problem in the past has been to model approximately and analytically the acceptance^{62,63}. While this can be readily implemented, a legitimate doubt can subsist about the accuracy of the experimental representation, especially in regions where edge effects might be important. In order to circumvent this problem, a numerical subroutine developed to reproduce the NA50 acceptance cuts and finite resolution effects in the measurement of muon pairs in Pb + Pb collisions at the CERN SPS was used⁶⁰. Thus, the invariant mass distribution of lepton pairs is computed in the hydrodynamic model, and then the pairs are run through the numerical detector simulation. The normalisation is determined by a fit to the Drell-Yan data using the MRSA parton distribution functions, as in the NA50 analysis. In order to get a p_T distribution, the dN/dM^2 estimates for Drell-Yan were supplemented with a Gaussian distribution in p_T ⁶², this very closely reproduces estimates obtained by the NA50 collaboration. The resulting invariant mass distribution is shown in Fig. 13. The p_T distribution is also computed. It is shown in Fig. 14. In

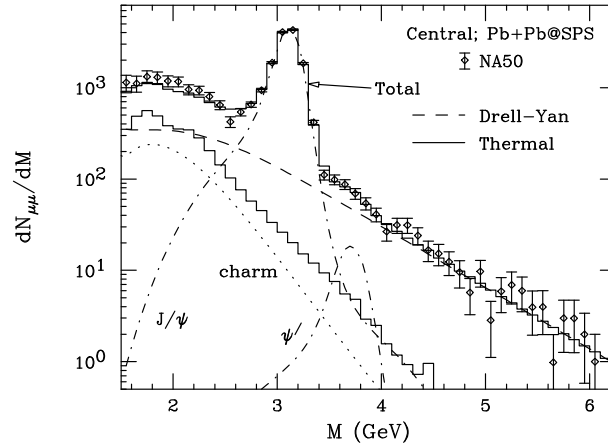


Fig. 13. The calculated dimuon invariant mass distribution, after correcting for the detector acceptance and resolution. The data are from the NA50 collaboration⁶⁴. The Drell-Yan and thermal contributions are shown separately, as well as those coming from correlated charm decay and from the direct decays of the J/ψ and ψ' .

both cases, good agreement with the experimental data is clearly achieved.

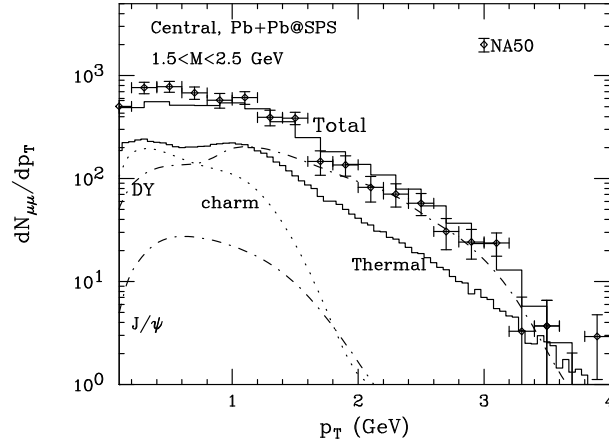


Fig. 14. The dimuon transverse momentum spectrum, after accounting for the detector effects. The data and the different curves are from the same sources as in Fig. 13.

As this point it is appropriate to consider the following question: which initial temperature is demanded by the intermediate invariant mass dilepton data? A critical and quantitative assessment of this issue can be obtained by examining a *linear* plot of the lepton pair mass spectrum in the region under scrutiny. This is shown in Fig. 15. From this figure it is clear that the best fit is provided by $\tau_0 = 0.2$ fm/c, and that the second best (less than two standard deviations away for most of the data points) belongs to $\tau_0 = 0.4$ fm/c. In terms of initial temperatures, those correspond to $T_0 \approx 330$ and 265 MeV respectively. A conservative and reasonable point of view is that it is probably not fair in such a challenging and complex environment as that of ultrarelativistic heavy ion collisions to ask for an agreement that is better than two standard deviations, considering all of the inherent uncertainties. The quark matter contribution (as modeled by $q\bar{q}$ annihilation) is $\approx 23\%$ for $\tau_0 = 0.2$ fm/c, and $\approx 19\%$ for $\tau_0 = 0.4$ fm/c, around a lepton pair invariant mass of 1.5 GeV.

Focus so far has been placed on high multiplicity data only. However, to extend the hydrodynamic model to non-central events and to properly treat the azimuthal anisotropy is not a simple task. However, one can get an approximate estimate of the centrality dependence by ignoring the broken azimuthal symmetry and by approximating the region of nuclear overlap by a circle of radius $R \approx 1.2 (N_{\text{part}}/2)^{1/3}$, where N_{part} is the number of participants^{65,60}. A centrality-dependence is generated thusly and shown

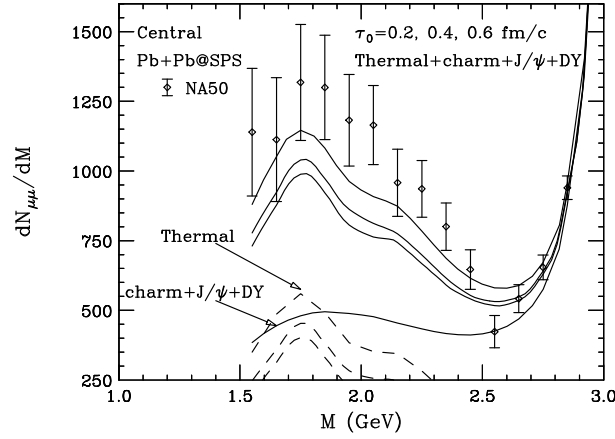


Fig. 15. A linear plot of the net dilepton spectrum in the intermediate mass region. The three solid curves correspond to formation time $\tau_0 = 0.2, 0.4, 0.6$ fm/c, from top to bottom, respectively. The data are from [64]. The thermal contribution and that for hard processes are shown separately.

in Fig. 16. It is seen that the agreement with the measured data is quite good

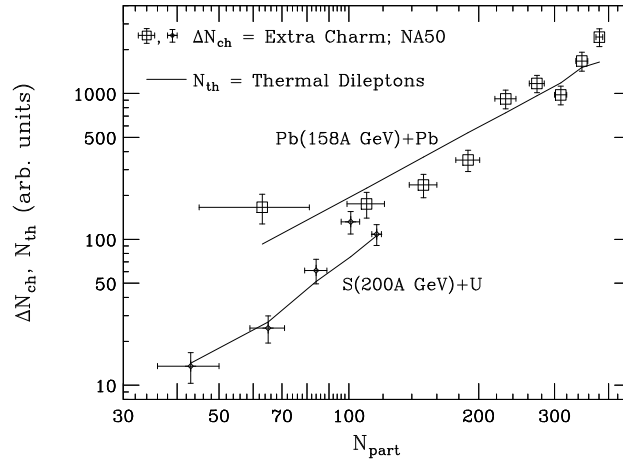


Fig. 16. Centrality dependence. The data represents the “extra charm” yield (as characterised by the NA50 collaboration⁶⁴) needed to describe the intermediate mass dilepton data. The solid curves are from the sources discussed in the text.

and that this approach gives a fair description of the centrality dependence

of the excess dilepton measurement.

What has been learnt from this exercise is that many-body channels, important in the low mass region, also still play a vital role in the intermediate mass domain. This unity is satisfying. It also happens that the global dynamical behaviour of the electromagnetic radiation can be empirically modeled⁶¹. Perhaps more importantly, the case where the data shown in this subsection are interpreted as the signature of a charm excess no longer appears to be very compelling. The findings described here are in agreement with previous calculations of dilepton radiation at this mass scale^{40,62}. As mentioned previously, the portion of the signal that emanates from the deconfined sector is around 20%, a figure that is unfortunately too small to support convincing claims of a QGP presence, once all uncertainties are factored in.

2.3. Photons

2.3.1. General Strategy

Real photons differ from previously discussed dileptons in a couple of important ways. First, they are on-shell and thus cannot be accommodated kinematically with two-hadron annihilation processes. From the beginning then, the only one-loop contributions to the current-current correlator (or retarded self-energy) are the hadronic radiative decays $\pi^0 \rightarrow \gamma\gamma$, $\eta \rightarrow \gamma\gamma$, and $\omega \rightarrow \pi^0\gamma$. Although the ω lifetime is ~ 23 fm/c and so that channel could be considered a thermal source (just barely), the others are clearly non-thermal sources with lifetimes much longer than the fireball. Such contributions must be considered in the overall yield, but are outside of the scope of the present discussion focusing on thermal emission. The one-loop contributions therefore play a smaller role in photon production as compared with dilepton production and consequently the discussion begins seriously here at two loops. Second, and something of a technical point, is that real photons have only two polarisation states over which to sum, rather than three as was the case for virtual photon propagation. In the same spirit then as the dilepton case, real photon emission from resonance hadronic matter can be most systematically studied by beginning with the photon self energy at two-loop order and working upward. The occupation numbers for the internal lines pay always a Boltzmann penalty and it is therefore natural to begin with the lightest species and with the minimum number of hadrons. As a aside remark, since the evaluation of two-loop topologies at finite temperature is technically challenging (although not

impossible), many photon rate calculations rely on a kinetic theory approach.

Since the energy regime is both relativistic and nonperturbative in terms of QCD degrees of freedom, it is commonplace to use effective theories for the composite hadron dynamics. Typically one starts with an effective Lagrangian with a large enough flavour symmetry to account for the lightest and relevant species. As a general rule, the pions are most important, followed by rho and so on, simply owing to increasing mass. Quantum numbers also play a role in terms of spin states and isospin states governing densities, and so one must be systematic. With interactions under some control relative to chiral symmetries, gauge invariance, conservation requirements of various sorts, one uses cutting rules on the two-loop self-energy diagrams in order to generate a list of reactions of the type $h_a + h_b \rightarrow h_1 + \gamma$ and $h_a \rightarrow h_1 + h_2 + \gamma$.

2.3.2. Establishing the Rates

The above mentioned strategy was first taken by Kapusta, Lichard and Seibert⁶⁶ where π - ρ and light meson dynamics were investigated. The dynamics were modeled with

$$\mathcal{L} = \frac{1}{2}|D_\mu \Phi|^2 - m_\pi^2 |\Phi|^2 - \frac{1}{4}\rho_{\mu\nu}\rho^{\mu\nu} + \frac{1}{2}m_\rho^2 \rho_\mu \rho^\mu - \frac{1}{4}F_{\mu\nu}F^{\mu\nu}. \quad (24)$$

Coupling of the rho and the photon to pions was accomplished with the covariant derivative $D_\mu = \partial_\mu - ieA_\mu - ig_\rho \rho_\mu$. The charged and neutral pions are embodied in the complex pseudoscalar field Φ , the vector rho and photon field strength tensors are respectively $\rho_{\mu\nu} = \partial_\mu \rho_\nu - \partial_\nu \rho_\mu$ and $F_{\mu\nu} = \partial_\mu A_\nu - \partial_\nu A_\mu$. Calibration is done by fitting the $\rho \rightarrow \pi^+ \pi^-$ decay rate with the choice $g_\rho = 2.9$.

The specific channels studied in Ref. [66] were dubbed annihilation $\pi^+ \pi^- \rightarrow \rho \gamma$ and “Compton scattering” $\pi \rho \rightarrow \pi \gamma$, and finally, neutral rho decay $\rho \rightarrow \pi^+ \pi^- \gamma$ (essentially the finite temperature analog of the vacuum process studied by Singer⁶⁷). Since the η meson mass is intermediate between pion and rho, its Boltzmann penalty is less than rho’s. Its effects were also considered by including the channels $\pi^+ \pi^- \rightarrow \eta \gamma$, $\pi^\pm \rightarrow \pi^\pm \gamma$. Owing mostly to coupling strengths (or weaknesses), these channels were found to be less important as compared to the purely π and ρ channels by more than an order of magnitude. Finally, in this initial study of photon production, the channel $\pi^+ \pi^- \rightarrow \gamma \gamma$ was included, though it was seen to contribute very little.

The matrix elements for all the processes enumerated above are included in Ref. [66] and will therefore not be repeated here. The energy dependent invariant rate for producing photons is then obtained by folding in Bose-Einstein (enhanced, if final) hadron distribution functions and Lorentz invariant phase space. For instance, for the channels $p_a + p_b \rightarrow p_1 + p_\gamma$, one has

$$E_\gamma \frac{dR}{d^3p_\gamma} = \mathcal{N} \int |\bar{\mathcal{M}}|^2 (2\pi)^4 \delta^4(p_a + p_b - p_1 - p_\gamma) \frac{d^3p_a}{(2\pi)^3 2E_a} f_a \\ \times \frac{d^3p_b}{(2\pi)^3 2E_b} f_b \frac{d^3p_1}{(2\pi)^3 2E_1} (1 + f_1) \frac{1}{(2\pi)^3 2}, \quad (25)$$

where \mathcal{N} is the appropriate degeneracy factor counting the states.

The resulting rates have been established numerically. However, analytical parametrisations valid for $100 \text{ MeV} < T < 200 \text{ MeV}$ and $0.2 \text{ GeV} < E_\gamma < 3 \text{ GeV}$ have been proposed^{68 a}.

$$E_\gamma \frac{dR}{d^3p_\gamma}(\pi\pi \rightarrow \rho\gamma) = 0.0717 T^{1.866} \exp(-0.7315/T + 1.45/\sqrt{E_\gamma} - E_\gamma/T), \\ E_\gamma \frac{dR}{d^3p_\gamma}(\pi\rho \rightarrow \pi\gamma) = T^{2.4} \exp(-1/(2T E_\gamma)^{3/4} - E_\gamma/T), \\ E_\gamma \frac{dR}{d^3p_\gamma}(\rho \rightarrow \pi\pi\gamma) = 0.1105 T^{4.283} E_\gamma^{-3.076+0.0777/T} \exp(-1.18 E_\gamma/T). \quad (26)$$

In these expressions, T is the temperature, E_γ is the photon energy; both must be reported in GeV. The numerical constants have appropriate units in each case and the numerical values out in front have units $\text{fm}^{-4}\text{GeV}^{-2}$. The numerical results are shown in Fig. 17.

The rate for the $\omega \rightarrow \pi^0\gamma$ is also included in Fig. 17. It can be written as^b

$$E_\gamma \frac{dR}{d^3p_\gamma}(\omega \rightarrow \pi^0\gamma) = \frac{3m_\omega^2 \Gamma(\omega \rightarrow \pi^0\gamma)}{16\pi^3 E_0 E_\gamma} \int_{E_{\min}}^{\infty} dE_\omega f_{BE}(E_\omega) \\ \times [1 + f_{BE}(E_\omega - E_\gamma)] \quad (27)$$

where $E_{\min} = m_\omega(E_\gamma^2 + E_0^2)/2E_\gamma E_0$, and E_0 is the photon energy in the rest frame of the ω meson.

^aThe process $\rho \rightarrow \pi\pi\gamma$ was slightly miscalculated in Ref. [66] owing to an omission of a Lorentz-boost factor. The parametrisation of the process published in Ref. [68] is therefore not optimal. A slightly different parametrisation is proposed here which correctly accounts for covariance effects.

^bNote that Eq. (54) of Ref. [66] has an incorrect Lorentz-boost factor. The formula has been corrected here and reported in Eq. (27).

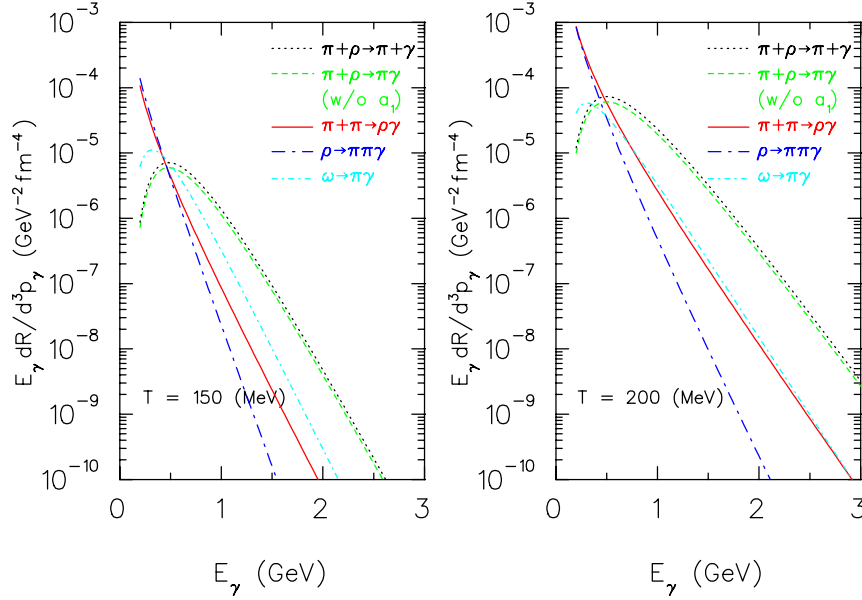


Fig. 17. Photon emission rates from Ref. [68] plus an estimate including the a_1 coherently. The $\omega \rightarrow \pi \gamma$ rate results from Eq. (27). Temperatures are fixed at $T = 150$ MeV and $T = 200$ MeV.

2.3.3. Refinements

Soon after these initial rate calculations were done, Xiong, Shuryak and Brown⁶⁹ pointed out that the a_1 meson would have an important effect on the $\pi \rho \rightarrow \pi \gamma$ channel. It is a resonance in the $\pi \rho$ sector with pole mass roughly matching the average \sqrt{s} in the fireball and with a rather large width ~ 400 MeV. An interaction for the $a_1 \pi \rho$ vertex was proposed, stemming not from some symmetry argument but rather, a vertex having minimal momentum dependence and still respecting gauge invariance. The idea was to set the scale as simply as possible for the contribution from this process. From the strong-interaction vertex, vector dominance was employed to subsequently describe radiative decay. The a_1 was indeed found to be important when studied this way—even dominating the other exchanges.

However, by itself the s -channel a_1 diagram does not carry complete information on the overall strength of the Compton process. Instead, a coherent sum of pion exchange and a_1 exchange was necessitated. Song⁷⁰

later carried out a study of photon production using a Chiral Lagrangian with vector and axial-vector fields introduced as dynamical gauge bosons of a hidden local symmetry. The role of the a_1 once again seemed to be important. However, Song found that fitting the relevant masses and coupling strengths in the model allowed two solutions, *i.e.* two parameter sets, and was therefore not able to uniquely identify an emission rate from this channel. It was later found, while studying dilepton emission with the same model, that parameter set II was the more reliable one in terms of its ability to match the observable hadronic quantities⁴³. In particular, the D/S ratio in the scattering amplitude for $a_1 \rightarrow \pi\rho$ was more closely respected with parameter set II. One thus observes a diminished presence of the a_1 meson (as opposed to estimates cited above) in the final rate. A modest enhancement of 20%, attributable to the pseudo-vector, is illustrated in Fig. 17. An update on this is forthcoming⁷¹. A study with the hidden local symmetry approach also points to a reduced role of the a_1 meson⁷².

Strange particles have been found to be only marginally important in the literature up to now. Specifically, the radiative decay $K_1 \rightarrow K\gamma$ was considered and was shown to be strong relative to the non-strange contributions only in a limited kinematic domain⁷³.

A final cautionary remark is in order here. When the rate spectra are studied at photon energies above 1 GeV, one must keep in mind that hadronic form factors have not been implemented in most of the rate calculations up to now (an exception is the Kapusta, Lichard and Seibert calculation⁶⁶ which estimated the form-factor effect on the $\pi\pi \rightarrow \rho\gamma$ channel), and could result in a suppression of a factor of 2 or more at higher photon energies. This is where the exchanged meson goes further off shell and brings forward possibly large form-factor effects. Advances in this direction will be important.

2.3.4. *Medium Effects*

In terms of higher-order effects, corrections to these rates come in at least two forms. First, there are off-shell effects which can be conceptualised by dressing the propagators and vertices for the internal hadron species in the general photon self-energy structure. These are the so-called form factors mentioned earlier in cautionary remark. Second, and beyond this, there are bona fide medium effects (finite temperature and density effects, *e.g.* width smearing and pole mass adjustments) that could be quite important. The typical pursuit in studies of medium modifications is to investigate the ef-

fects of dramatic collision broadened vector meson spectral distributions⁷⁴ and/or the dropping of the rho mass according to the so-called Brown-Rho scaling⁷⁵ or some other ansatz. Several authors have studied various pieces of the overall medium dependences^{76,77,78,72}. The trends are the following. While the in-medium vector meson widths are expected to be rather large, the effect on photon production is not too significant. This makes sense since the vector spectral distributions contribute to photon production only as an integral over the specific distribution—and smearing the distribution does not affect the normalisation. Mass shifts, on the other hand, have been shown to affect the rates by anywhere from a factor of 3 up to an order of magnitude^{76,77}. The results are too model dependent to make specific concluding statements at present.

2.3.5. *Alternative Approach: Chiral Reduction Formulae*

Instead of computing photon production rates using a channel-by-channel assessment, Steele, Yamagishi, and Zahed used chiral reduction formulae together with a virial expansion and they came forward with photon and dilepton emission rate estimates. The general idea is that the invariant production rate is proportional to the trace over a complete set of hadronic states of the hadronic (Boltzmann weighted) Hamiltonian convoluted with a current-current correlator. The hadronic part of the correlator is written as a virial type expansion truncated in a particular way. The expansion coefficients are constrained by various general arguments, *e.g.* broken chiral symmetry, unitarity, and gauge invariance and also, when available, constrained by observed spectra: electroproduction, τ decay, radiative pion decay, and so on. The thermal photon emission estimates in this approach tend to be larger than those using an effective Lagrangian approach by a factor of 2–4^{79,80}. At present, this might be the honest theoretical error bar in the rate estimates even after a decade of model calculations. Progress continues especially with effective theories in the hadronic matter converging with results from models firmly rooted in QCD as the fundamental degrees of freedom as discussed in the next section. This is the so-called duality of hadronic matter and quark matter at the phase boundary that one expects.

At this stage in the discussion it is somewhat premature to integrate the photon production rates over a space-time evolution, which would then facilitate a comparison with experiment, because radiation from partonic matter has not yet been discussed. So, before considering photon yields

from nuclear collisions and making contact with data, the partonic contributions to electromagnetic radiation will be presented, and then yields will be discussed.

3. Radiation from Partons

It is of great theoretical importance to establish the production rates of electromagnetic radiation for many-body systems beyond the deconfinement phase boundary of nuclear matter. A model is employed whereby the matter is assumed to be fully in the partonic phase. Whilst experimental verification of an unequivocal identification of thermalised quark-gluon plasma is still forthcoming, it is the appropriate picture with which to work as a baseline. The general formalism established for photon production rates from hadronic matter in Sect. 2 is generic to all quantum field theories and is thus equally valid for partonic degrees of freedom. And yet, the massless nature of the up and down quarks requires special attention. Computational tools known as hard-thermal-loop (HTL) methods have been applied to handle infrared singularities. Independent of the experimental advancements then, it would already be important to establish quark matter radiative emissivities. Since heavy-ion experiments at the CERN SPS and at RHIC have most likely probed into small areas of the deconfined region in the nuclear matter phase diagram, there is further motivation, and indeed some urgency, for theoretical investigations to converge and to report emission rates. Therefore, the status of theory for photon production from finite temperature quark matter is discussed below and a separate section is devoted to dilepton production.

3.1. Photons

The imaginary parts of one-loop contributions to the photon self-energy, obtained with appropriate cuts, are identically zero due to vanishing phase space. Certain two-loop diagrams give nontrivial contributions. Cutting rules provide a bridge between kinetic theory and field theory where in fact, a mapping has been established⁸¹. The result of cutting two-loop diagrams gives QCD processes of the types $q\bar{q} \rightarrow g\gamma$ and $qg \rightarrow q\gamma$ or $\bar{q}g \rightarrow \bar{q}\gamma$. These processes, as well as bremsstrahlung processes, were studied using perturbative matrix elements two decades ago^{82,83,84}. The results were unfortunately infrared unstable (*i.e.* the rates diverged as the quark mass tended to zero). Significant improvement came when the “annihilation” and “Compton” processes were analysed by Kapusta *et al.*⁶⁶ and Baier *et al.*⁸⁵

using resummation techniques of Braaten and Pisarski^{86,87}. The basic idea behind the resummation technique, or the so-called hard-thermal-loop approximation, is that weak coupling at high temperatures allows a separation of scales, and a separation of the rate into soft (quark momentum $\sim gT$ or smaller) and hard (quark momentum T or larger) contributions. The soft contribution can be computed with an appropriately dressed quark propagator in the one-loop photon self-energy, while the hard contribution can be computed using perturbative methods and kinetic theory. In each result, the separation scale appears as a sort of regulator. When the soft plus hard contributions are collected together and added, the result is independent of the separation scale, and of course also independent of quark mass since it was set to zero from the beginning. The exact result can be established only numerically. However, using an approximation which is valid for $E_\gamma/T \gg 1$, a simple pocket formula has been proposed. At the time, this result was thought to be complete to order $\alpha\alpha_s$. Specialising to two quark flavours the result is

$$E_\gamma \frac{dR}{d^3p_\gamma} = \frac{5}{9} \frac{\alpha\alpha_s}{2\pi^2} T^2 e^{-E_\gamma/T} \ln \left(\frac{2.912}{g^2} \frac{E_\gamma}{T} \right). \quad (28)$$

A value of $\alpha_s = 0.4$ ($g^2 = 5$) is used and a “1” is added to the argument of the logarithm when plotting as suggested by Kapusta *et al.* to more closely match the exact numerical result for photon energies of the order of the temperature. This also ensures the rate is always positive. These results were subsequently generalised to finite quark chemical potential and also applied to chemical non-equilibrium systems. For a discussion of these effects see [88] and references therein.

Having photon emission rates from QCD free from infrared instability ailments represented significant advancement and was at the time, thought to be the *complete* lowest order result. After all, the two loop contributions to the self-energy (that is, the dressed two-loop contributions, which actually contain arbitrarily many loops) seem naively to contribute to photon production at $\mathcal{O}(\alpha\alpha_s^2)$. They specifically correspond to bremsstrahlung processes and annihilation with scattering. The extra vertices would introduce an extra power of g^2 as compared with the one-loop result. However, Aurenche *et al.* showed that the two-loop HTL contribution is curiously not of higher order, but instead contributes to order $\alpha\alpha_s$ too⁸⁹. This owes essentially to a collinear singularity when the exchanged gluon is soft. The resummed gluon propagator introduces a g^2 in its denominator which cancels the “extra” g^2 from the additional vertices. The overall contribution

to the HTL for this category of two-loop diagrams is the same (lowest order in $\alpha\alpha_s$). In terms of the kinetic theory analog, these correspond to such processes as $q\bar{q} \rightarrow g\bar{q}\gamma$, $gq \rightarrow gq\gamma$, and $q\bar{q}q \rightarrow q\gamma$, or $q\bar{q}g \rightarrow g\gamma$ (and still others with antiquarks). Two- and even three-loop contributions were shown to contribute to lowest order, and the rates continued to rise!

It is fair to say that after these features were pointed out by Aurenche *et al.*, the situation appeared to signal a breakdown in perturbation theory for finite temperature QCD. However, it has been shown recently by Arnold, Moore and Yaffe that as long as $E_\gamma \gg gT$, there is sufficient cancellation due to many-body effects so that the lowest-order rate is identifiable and fully under control⁹⁰. This remarkable result represents a significant advancement in this field. There were unfinished details within the topics of bremsstrahlung⁸⁹, magnetic mass⁹¹ and coherence effects⁹² that Arnold *et al.* resolved by analysing multiple-loop ladder diagrams which introduce multiple scattering interference effects of Landau-Pomeranchuk-Migdal (LPM)^{93,94}. A digression will not be taken here to reproduce the lengthy and specialised argument, but the result is the following. The suppression is sufficient to regulate the rates because 1-loop, 2-loop and multiple-loop diagrams can be consistently resummed to give a finite rate! The efforts of many people over a decade of work have produced a complete photon production calculation from QCD to lowest order $\mathcal{O}(\alpha\alpha_s)$. The simple expression below parametrises the exact numerical solution for two quark flavours.

$$E_\gamma \frac{dR}{d^3p_\gamma} = \frac{5}{9} \frac{\alpha\alpha_s}{3\pi^2} T^2 \frac{1}{e^{E_\gamma/T} + 1} \times \left[\ln\left(\frac{3T}{g}\right) + \frac{1}{2} \ln\left(\frac{2E}{T}\right) + C_{2\rightarrow 2} + C_{\text{brem}} + C_{\text{annih}} \right], \quad (29)$$

where

$$C_{2\rightarrow 2} \simeq 0.041(T/E_\gamma) - 0.3615 + 1.01e^{-1.35E_\gamma/T}$$

$$C_{\text{brem}} + C_{\text{annih}} = \frac{0.633 \ln(12.28 + (T/E_\gamma))}{(E_\gamma/T)^{3/2}} + \frac{0.154(E_\gamma/T)}{\sqrt{1 + (E_\gamma/16.27T)}}. \quad (30)$$

Results are shown in Fig. 18, where a value for the strong coupling $\alpha_s = 0.4$ ($g^2 = 5$) is used as before, and superimposed onto the total hadron rate discussed previously. The striking feature is that after the dust has settled on the QCD calculations, with HTL to 1-, 2-, and even multiple-loop order, with LPM effects carefully included, the QCD rate at fixed temperature is once again the same as the hot hadronic gas rate. The QGP and the hadron gas seem to “shine just as brightly”.

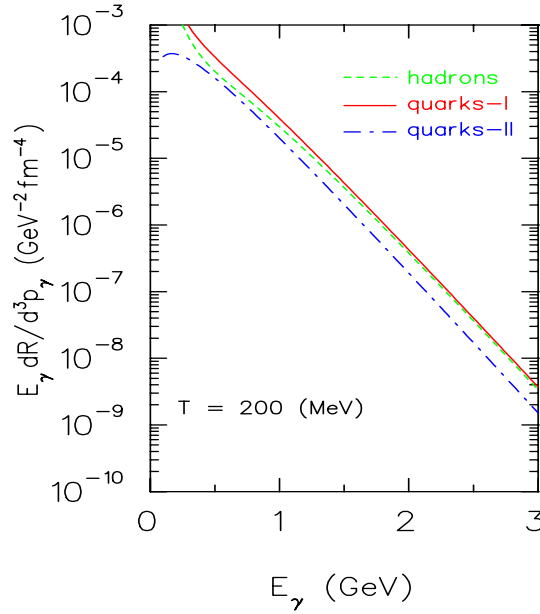


Fig. 18. Photon emission rate for QGP from Kapusta *et al.* in Ref. [66] (labelled Quarks-II) and Arnold *et al.* in Ref. [90] (labelled Quarks-I). Quarks-II includes Compton and annihilation, while Quarks-I includes in addition, bremsstrahlung and certain $3 \rightarrow 2$ processes. Quarks-I is the “complete lowest order calculation”. Temperature is fixed at $T = 200$ MeV. Total hadron contribution is also displayed for comparison purposes.

3.1.1. Photon Measurements

Photon experiments using heavy-ion beams are notoriously difficult and signals of any kind are already a notable accomplishment. At high energies, there are at present two sets of data with which to compare the theory. The WA80 collaboration at CERN first reported and discussed their yields as absolute measurements, but were later forced to loosen the constraints somewhat and suggest upper limits only. Their direct photon limits came from 200A GeV $^{32}\text{S} + \text{Au}$ collisions⁹⁵. Secondly, the WA98 collaboration measured direct photons in 158A GeV $^{208}\text{Pb} + ^{208}\text{Pb}$ collisions also at CERN⁹⁶. The hope from the onset was to challenge the theory using production rates convoluted with a temperature profile evolving according to one of two possible scenarios: 1) the system first comes into equilibrium well above the phase boundary and therefore the quark rates contribute until such time as the system reaches the mixed phase. Overlapping four volumes mean that quarks and hadrons contribute until the latent heat is

absorbed fully into a hadronic state, and finally, the hadrons emit until freezeout; and scenario 2) where the system reaches a very hot and dense hadronic state and simply radiates photons while cooling and eventually freezes out. The burning question is which scenario is consistent with the measurements? Can either one be ruled out?

There were several attempts to describe the WA80 results and do just that. Shuryak and Xiong⁹⁷ first used the hadron rates with their version (incoherent treatment) of a_1 meson dynamics included, and their conclusion was that the excess photon signal could not be described with a conventional expansion scenario. They consequently suggested a long-lived mixed phase as a possible explanation. Since the data were later reported as upper limits only, the conclusion no longer rested on strong experimental support.

Srivastava and Sinha applied the quark rates at the 1-loop HTL level and the hadron rates comparing scenarios (I) with and (II) without a phase transition to QGP⁹⁸. They argued that the data (which later became upper limits) are well described by a scenario where QGP is formed initially. Bjorken hydrodynamics was employed with $T_i = 203$ MeV, $T_c = 160$ MeV, and $T_f = 100$ MeV for scenario (I) and, $T_i = 408$ MeV for scenario (II). Other models came forward attempting to describe the experimental results. For example, Dumitru *et al.* used a three-fluid hydrodynamics without and with a phase transition⁹⁹. They came to similar conclusions, that without a phase transition to quark matter, the results were inconsistent with experiment.

Improvements in rate calculations from quark matter brought advancement also in yield estimates. Two-loop HTL rates were coupled with hydrodynamics, and then later corrected due to numerical errors along the way¹⁰⁰. The most recent and corrected comparison of the WA80 upper limits to hydrodynamic model estimates are displayed in Fig.19. The conclusion is that both scenarios, without and with a phase transition, seem to be consistent with the upper limits. A more complete hadronic equation of state (EOS) and up-to-date photon rates from quark matter lead to these new conclusions.

With the WA80 results in hand and even anticipating the forthcoming WA98 data at that time, Cleymans, Redlich and Srivastava¹⁰¹ used a hydrodynamical model, which arguably provided better description of the evolution as compared to previous model calculations and, in particular, could more completely describe the transverse flow likely to be generated at the SPS. The initial QCD rates of Kapusta *et al.* were used and the hadron rates, including the effects of the a_1 meson, were implemented with

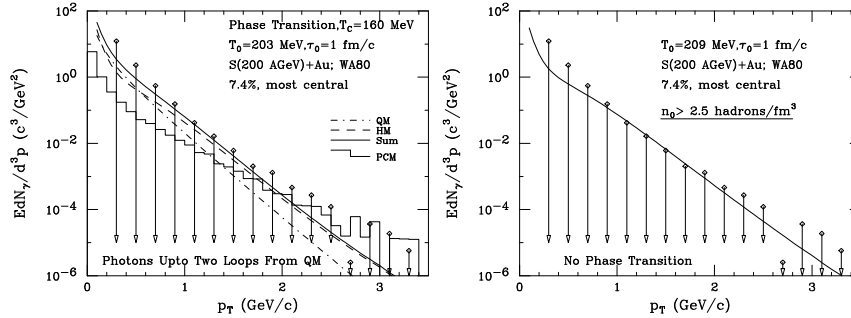


Fig. 19. Upper limits at the 90% confidence level from WA80 on the invariant excess photon yield per event for the 7.4% σ_{mb} most central collisions⁹⁵ as compared with hydrodynamical models with (left) and without (right) phase transition

all hadrons up to 2.5 GeV mass contributing to the equation of state. They concluded that while the final yields were not significantly different in a QCD plus hadron matter scenario as compared with a fully hadronic picture, they argued that the physics seemed to favour the former since in the hadronic picture particle densities were beyond anything reasonable for hadronic language to be justified.

Before moving to the WA98 data, one might make the remark that since the WA80 results are upper limits rather than measurements, and due to the uncertainties in the theoretical production rates and, mostly, with the uncertainties in the models for the evolutions of the nuclear systems, no definite conclusions can be reached.

The eagerly anticipated direct photon measurement from $^{208}\text{Pb} + ^{208}\text{Pb}$ collisions at 158A GeV were published in 2000 by the WA98 collaboration⁹⁶. The collaboration presented their data as compared with several proton-induced reactions at similar energies and scaled up to central $^{208}\text{Pb} + ^{208}\text{Pb}$ collisions. For $p_T > 1.5$ GeV, where the signal is strongest, there is a clear excess beyond that which is expected from proton-induced reactions. In other words, the results are quite suggestive of thermal photon emission, or perhaps pre-equilibrium emission. One contribution that is non-negotiable in those data is that due to perturbative QCD. It owes its existence to collisions during the first instants of the reaction, and should appear in pp, pA, and AA measurements. The WA98 data is shown in Fig. 20, along with a pQCD estimate¹⁰². Even though the presence of pQCD effects at the energies under discussion here can't be argued against¹⁰³, the

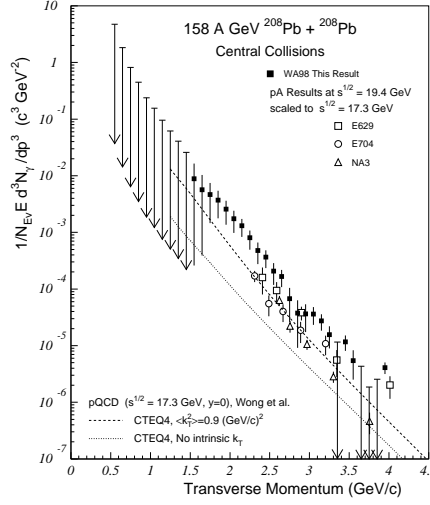


Fig. 20. The WA98 real photon measurements as a function of photon transverse momentum. The pQCD estimates are from [102].

application to nucleus-nucleus data contains some ambiguities that need to be pointed out in order to make progress. Specifically, it is clear that some amount of parton intrinsic transverse momentum (neglected in strict NLO calculations) should manifest itself. Simple uncertainty principle arguments support this²⁹, and soft gluon emission should increase the value further¹⁰⁴. However, attempts to extract meaningful values from experiments have remained inconclusive; for example a recent survey found that fixed target data at ISR energies ($\sqrt{s} \leq 23$ GeV) were inconsistent¹⁰⁵. Furthermore, in nucleus-nucleus collisions, a part of the parton transverse momentum can be ascribed to multiple soft scattering of the nucleons prior to the hard scattering¹⁰⁶, and this has to be modeled dynamically and independently. It is important to note that, at RHIC, several of those uncertainties will be lifted, as measurements of pp, pA, and AA reactions will be performed *at the same energy* with identical detector configurations. Bearing all those caveats in mind, a recent study¹⁰⁷ of E704 and WA98 data found that $\langle k_t^2 \rangle \simeq 1.3$ GeV² could be extracted from pp reactions, leaving up to 1 GeV² for nuclear effects. This analysis is shown in Fig. 21. It is clear from this work that photon transverse momenta below 2.5 GeV are under-predicted by this pQCD estimate. Also, around this momentum,

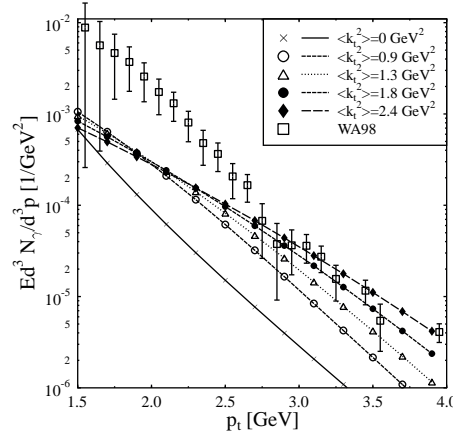


Fig. 21. The WA98 data with pQCD estimates of transverse parton momentum. From [107].

the exact value of the intrinsic transverse momentum ceases to be important. A softer component of the photon spectrum is called for, and this will be discussed shortly. Note that this value for a separation of scale between the “hard” and “soft” photon sources also appears if one fits the high momentum pQCD spectrum to the data, with a K factor^{108,61}. It is argued in these cited works that the soft component possesses thermal characteristics.

Srivastava and Sinha¹⁰⁹ studied mechanisms for excess photon production using an hydrodynamic expansion applied to the $^{208}\text{Pb} + ^{208}\text{Pb}$ system. The photon emission rate from quarks was input using the result from two-loop HTL calculations from Aurenche *et al.*⁸⁹. However, it is probably fair to say that those rates have been superseded by the calculations in Ref. [90], which incorporates higher loop topologies and thus LPM effects. Production rates from the hadronic phase were taken from the parametrisation of Kapusta *et al.* plus an incoherent a_1 -exchange contribution to the process $\pi\rho \rightarrow \pi\gamma$. The results obtained there are shown in Fig. 22. The high initial temperature in this work is needed to generate a sufficient high transverse momentum component of the photon spectrum. In this respect, the WA98 data has been used to extract phenomenologically an initial radial veloc-

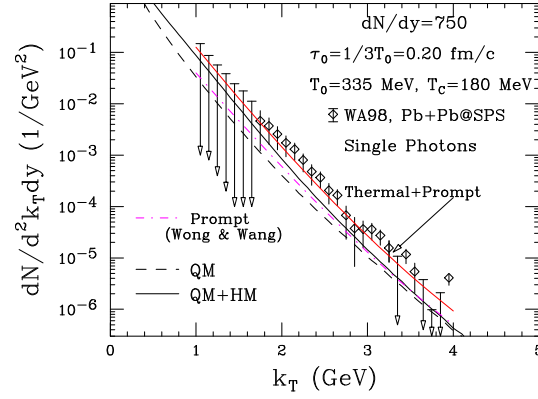


Fig. 22. Single photon production in Pb+Pb collisions at relativistic energies. For specific model details, consult Ref. [109].

ity profile¹¹⁰. The result of that study is shown in Fig. 23. Both of those theoretical efforts concluded that the excess seemed to be consistent with a thermal source of photons at roughly ~ 200 MeV temperature, while detailed and quantitative conclusions on a partonic scenario versus hadronic with strong flow were not definitively reached.

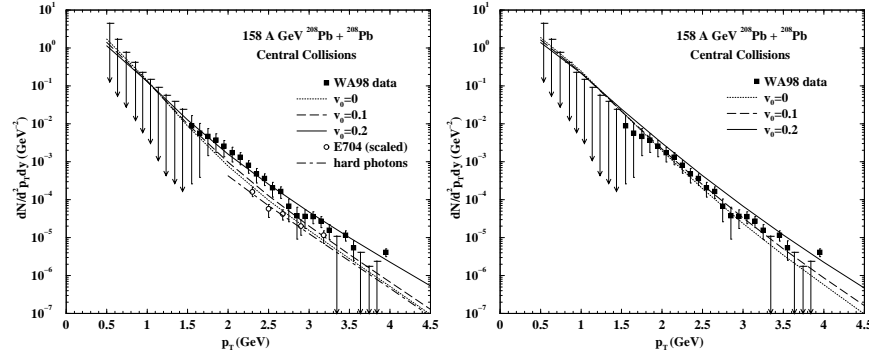


Fig. 23. Total photon yields from quark matter plus hadronic matter (left panel) and hadronic matter with medium-modified vector meson properties (right panel). The figure is reproduced here from Ref. [110].

Ruuskanen and collaborators also used hydrodynamics to compare theory with experiment^{111,112,113}. These workers have challenged hydrodynamics to find consistency with not only photon spectra, but also hadron and dilepton spectra—all within the same model and simultaneously. They also insist on reproducing the longitudinal hadron characteristics¹¹³. Several equations of state and therefore several expansion scenarios seem to describe the photon spectra and hadron spectra equally well. The degeneracy between the different equations of state and initial conditions is not lifted empirically, even though the data do require a high density and temperature initial phase.

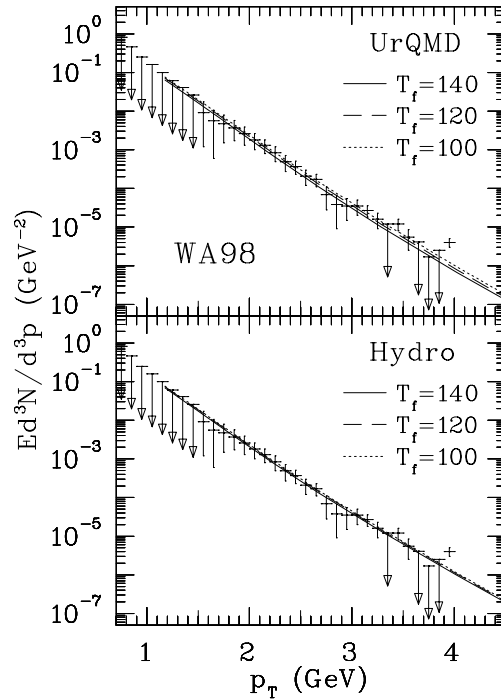


Fig. 24. Comparison of the WA98 photon spectrum to the predictions of the UrQMD model and the hydrodynamic model at several freezeout temperatures from Ref. [25].

A comparison of space-time models in reference to the WA98 data was recently carried out by Huovinen, Belkacem, Ellis and Kapusta²⁵ wherein hydrodynamics and a course-grained UrQMD were used to produce photon spectra (dilepton spectra were also calculated within theory and compared

to experiment). Notably, the “complete” lowest order photon production rate [$\mathcal{O}(\alpha\alpha_s)$] from the quark phase was used in this work. The basic conclusions were that UrQMD and hydrodynamics seem to give roughly the same qualitative features of expansion and cooling (although quantitatively, UrQMD cools more slowly due presumably to viscous and heat conduction effects); they give therefore, very similar results for photon production. The precise choice of freezeout temperature seemed to be irrelevant, indicating that the high temperature part of the evolution dominates photon production. Results are shown here in Fig. 24. The agreement between theory and experiment was described by these authors as “excellent”, while they reminded the reader that the rates have uncertainties and the initial conditions which were fed into the models are responsible for further uncertainties propagating to the final spectra.

A partial summary of the photon analyses is justified. It is an accurate statement that definite conclusions are elusive. Many physical ingredients have been invoked in the studies of heavy ion photon data, as seen above and in the quoted reviews, but uncertainties in many of those ingredients (if not all) preclude a clear interpretation of a signal that relies on a combination of their effects. But one example is the absence of the chemical potentials in hydrodynamics-based approaches. Another is the uncertainty in the basic photon rates. However, those uncertainties have narrowed down considerably in recent years, and this is true for rates in both the partonic and confined sectors. Also, as mentioned previously, the fact of being able to access data at the same energy in pp, pA, and AA events will make RHIC a fertile testing ground for theoretical models, and should allow the community to make more progress in differentiating between them.

3.2. *Dileptons*

The yield of low mass dileptons ($M < m_\phi$) from thermal quark-antiquark annihilation is not expected to be a great competitor of the two-pion annihilation simply owing to longevity effects in the two phases. The quark phase occupies a smaller four volume. Nevertheless, it is useful to assess the production rates as a benchmark and then to ask about higher-order corrections, especially in the medium. For high enough system temperatures, and for large enough invariant masses, $q\bar{q} \rightarrow \gamma^* \rightarrow e^+e^-$ is considered a more significant source and in terms of theory, can be reliably computed in a HTL approximation. The lowest order contribution [$\mathcal{O}(\alpha_s^0)$] in field theory language corresponds to a one-loop graph with bare quarks occupying

the internal lines. The imaginary part of the self-energy describes precisely the annihilation process mentioned above. The production rate is roughly the square of the density of quarks times the cross section times the relative velocity. These are now textbook formulae¹¹⁴ so one simply quotes the results

$$\frac{dR}{dM^2} = \mathcal{N} \frac{5}{9} \frac{\sigma(M)}{2(2\pi)^4} M^3 T K_1(M/T), \quad (31)$$

where the annihilation cross section is

$$\sigma(M) = \frac{4\pi}{3} \frac{\alpha^2}{M^2}, \quad (32)$$

and where \mathcal{N} is an overall degeneracy factor (24 when using two quark flavours) and finally, K_1 is the modified Bessel function of order 1. Here the quark and lepton masses have been set to zero. To compare the resulting rate with major hadronic contributors, Fig. 25 is presented. Already here, one sees that the Born term is not negligible and the natural next question is the role of higher order contributions.

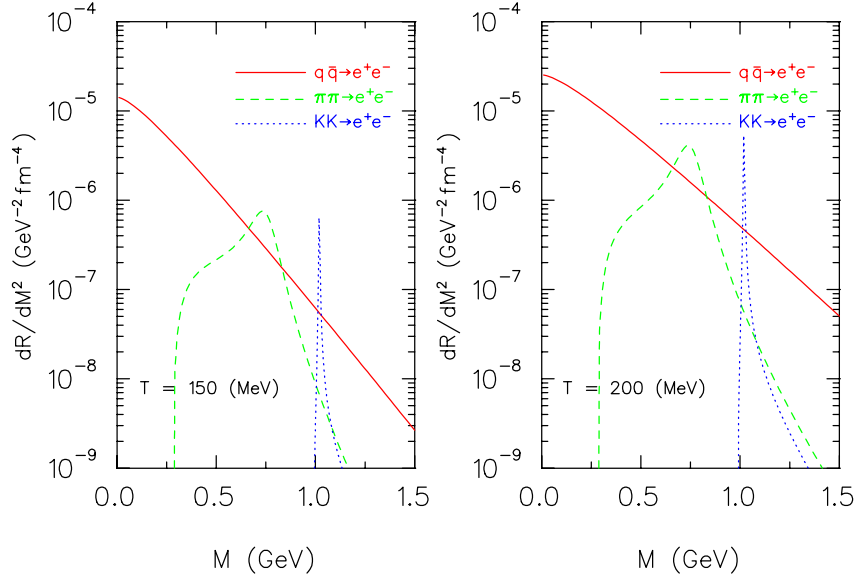


Fig. 25. Thermal production rate for dileptons via lowest order quark-antiquark annihilation as compared to leading hadronic channels $\pi\pi \rightarrow e^+e^-$ and $KK \rightarrow e^+e^-$. The temperatures are set to $T = 150$ MeV (left) and 200 MeV (right).

Perturbative corrections to these annihilation rates were considered by Braaten, Pisarski and Yuan¹¹⁸, who found that for very soft dileptons at rest in the medium (energies $\ll 1$ GeV) the corrections were orders of magnitude larger than the Born term. Also, unique structures emerged in these corrections owing to Van Hove singularities arising from significant softening of the quark dispersion relation in medium. There appears a minimum in the medium-modified quark dispersion relation (a plasmino) typically at dilepton energies less than that set by the quark mass. While these effects are quite intriguing, finite imaginary parts in the quark propagators and finite three-momentum effects for the dilepton¹¹⁹ could dampen the peaks into undetectable artifacts. Also, the softer bremsstrahlung contributions¹²⁰ might overshadow these total annihilation channels. For a review of these and other issues for the dilepton channels, see Ref. [24] by Rapp and Wambach.

Quark-antiquark annihilation is of course not the only relevant parton process for dilepton production. For instance, the $2 \rightarrow 2$ real photon production processes considered previously contribute also to lepton pair emission. In addition, there are annihilation processes where one of the incoming partons has already scattered and suffered an off-shell interaction. The resulting $3 \rightarrow 2$ process comes from off-shell annihilation (also called annihilation with scattering). Such mechanisms have been shown to dominate at high enough photon energy. Since this is essentially a many-body initial state, formation time considerations and coherence effects for the virtual photon suggest once again that multiple scattering plays an important role. Aurenche, Gélis, and Zaraket¹²¹, and together with Moore¹²², have applied the HTL technique for lepton pairs with $E/T \gg 1$ (either low mass but high momentum, or high mass) and have shown that the two-loop contributions which include bremsstrahlung of a quark and annihilation with scattering, are free from infrared and collinear singularity effects. When added to the Born term, the rescattering corrections plus the $2 \rightarrow 2$ processes^{123,124} result in a rate that is somewhat increased as compared with just the Born terms. Furthermore, threshold effects at $M^2 = 4m_q^2$ (thermal quark mass) are smoothed out, all of which is illustrated in Fig. 26.

The dilepton results from QGP discussed above assume equilibrium and use asymptotic values for such quantities as thermal quark masses and screening masses. Strictly speaking, these are only valid at asymptotic values of temperature: the assumptions needed for the theoretical machinery to remain consistent might actually break down at terrestrial accelerators

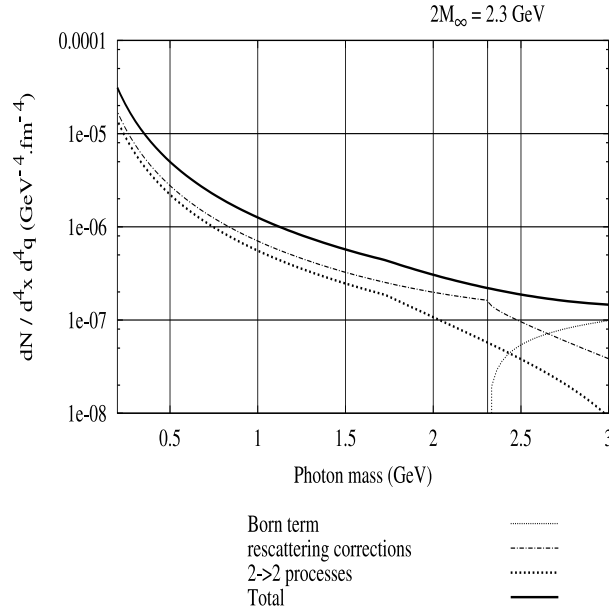


Fig. 26. The dilepton production rate per unit four momentum at fixed energy as a function of photon mass (dilepton mass). Values are fixed at $T = 1 \text{ GeV}$, $q_0 = 5 \text{ GeV}$, $\alpha_s = 0.3$ and two quark flavours were considered. The figure is reproduced here from Ref. [122].

energies. Scenarios more realistic for RHIC and LHC could be studied if alternative schemes were used to compute masses in nonperturbative circumstances. First steps in the direction of lattice evaluations of thermal dileptons using maximum entropy methods¹²⁵ have recently been taken¹²⁶.

4. Predictions

4.1. Photons

RHIC has been running, looking primarily at hadronic observables probing the later stages of ultrarelativistic nuclear reactions. Electromagnetic spectra will soon be available which, of course, probes deeper into the fireball and indeed cleanly into early stages of the reactions as well. Predictions for measurements of electromagnetic signals at RHIC are therefore very important. In addition, the Large Hadron Collider (LHC) is only five years away! While this number probably needs an appropriate error bar, it will soon become crucial to have formulated a set of model estimates for LHC

experiments too. A section is devoted here to discussing these sorts of predictions.

As one moves away from SPS systems and energies and goes to RHIC, and to LHC energies, there are increasing uncertainties in estimates for the initial energy densities. The initial state is very far from under control. But, as in all cases, when theory is extrapolated to new territory, the simplest estimates are first used to set the scales and subsequent to this, refinements and various improvements are made. It is in this spirit that photon production (yields) were recently estimated at RHIC and LHC by several authors^{110,127,128,129}. Simple 1+1 dimensional models show dominance of the QGP over the hadron gas for photon $p_T \gtrsim 3$ GeV (RHIC) and roughly 2 GeV (LHC)¹²⁹. Transverse expansion, which builds up particularly later in the hadron phase, makes distinction less clear, but the QGP might still outshine the hadron gas. The results for photon production from Ref. [129] are displayed in Fig. 27.

However, agreement is far from complete on this issue. For instance, Hammon *et al.*¹²⁷ predict that QGP will not be visible at RHIC owing to a very strong contribution from prompt photons (a pre-equilibrium source which has not been discussed here, and one which is probably not entirely under control), while at LHC the situation is different where QGP will be visible for limited photon kinematics. They used $T_0 = 533$ MeV (300 MeV) and $\tau_0 = 0.12$ fm/c (0.5 fm/c) for QGP (hadron gas) at RHIC, and they used $T_0 = 880$ MeV (650 MeV) and $\tau_0 = 0.1$ fm/c (0.25 fm/c) for QGP (hadron gas) at LHC. One could however hope that the prompt photons due to pQCD could be measured separately (in pp collisions at the same energy, for example), and subtracted out. Alam *et al.*¹¹⁰ find, using less extreme initial condition parameters (lower initial temperatures), that thermal photons will be visible for $p_T < 2$ GeV. However, they also find that thermal photons from hot hadronic gas populate the high p_T region even fairly strongly. Again, this is due to a strong flow built up later in the hadron phase.

In the face of such lack of agreement, which owes essentially to large uncertainties in the initial conditions, in the nature of the expansion, and even in the quark and hadron rates themselves, one suggests that it is premature to make any definite statement at this point. In other words, the theoretical error bar is too large at present to formulate any physics conclusions from photons. And yet on the optimistic side, theory will progress when the newest QCD rates and hadronic rates are implemented into a dynamical model which attempts to describe the buildup of collective flow

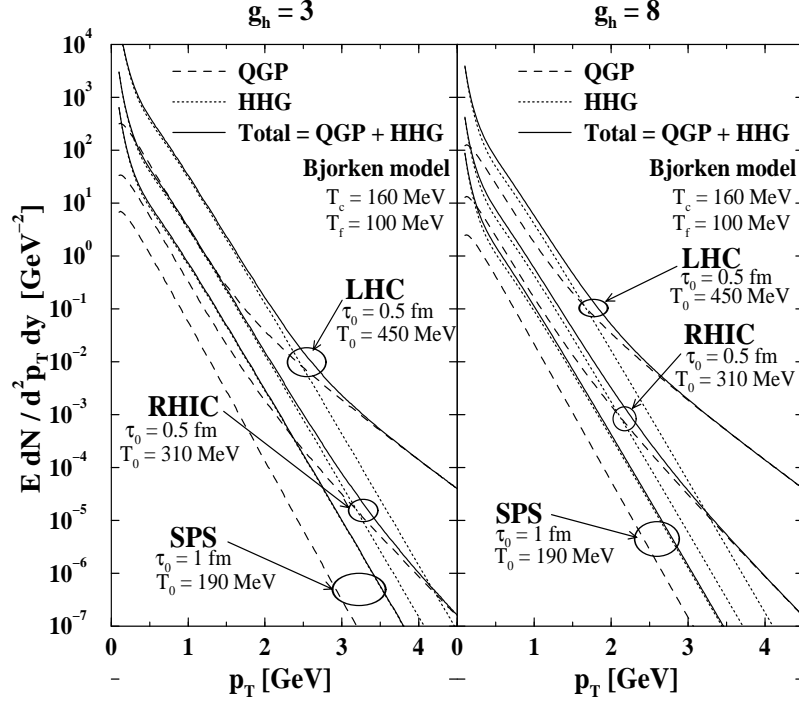


Fig. 27. Photon spectra (yields) from SPS, to RHIC, and LHC from Pb+Pb collisions. Two cases are shown, an ideal pion gas with $g_h = 3$ (left) and 8 (right) panels.

in some detail, on a species-by-species basis (viz. heavier species seem to flow differently from lighter ones).

In almost all cases discussed in this work, the dynamical simulations used to model the dynamics of nuclear collisions assume some form of equilibrium. Many approaches assume both chemical and thermal equilibrium, while some only need the latter ingredient. There exists, however, a whole class of models that attempt an *ab initio* rendering of the heavy ion reactions. Those are currently the only window one has to the very early stages of the collisions, and thus they potentially offer precious insight on the importance of pre-equilibrium generation of electromagnetic radiation. At ultrarelativistic energies, the degrees of freedom that appropriately describe this phase are partonic. A recent prediction of the photon yields has been made¹¹⁵, using a version of the parton cascade model (PCM)^{116,117}. Along with gauging the importance of the above-mentioned

pre-equilibrium effects, this calculation involves the application of perturbative QCD (pQCD) in a domain not necessarily restricted to large momentum transfers. The photons there are produced from Compton, annihilation, and bremsstrahlung processes at the parton level. All lowest-order QCD scatterings between massless quarks and gluons are included in this model. The obtained photon spectrum for the collision of gold nuclei at RHIC is shown in Fig. 28. There, the contribution from interactions involv-

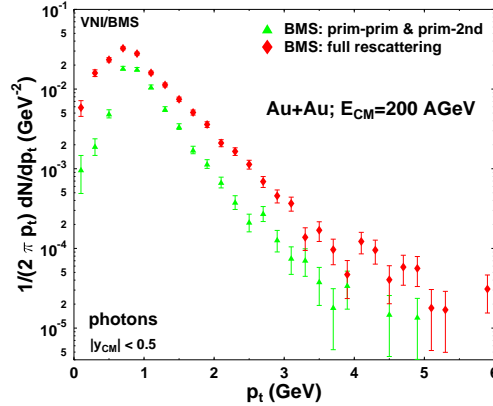


Fig. 28. Transverse momentum spectrum of photons from central collisions of gold nuclei at RHIC, calculated with the VNI/BMS parton cascade model¹¹⁷ (see the text for an explanation of the symbols).

ing at least one primary parton (triangles) is compared with that obtained with full binary cascading (diamonds). Most of the photons between 2 and 4 GeV have their origin in the multiple semi-hard scattering of partons. This finding would support the claim that high energy quarks going through a quark gluon plasma would yield electromagnetic signatures (see later sections).

4.2. Dileptons

The plasma signature in the lepton pair channels is expected to manifest itself mainly in the so-called intermediate mass sector³¹ (see Section (2.2)). Owing to the large multiplicities germane to the collider conditions, a large background will render the extraction of any direct electromagnetic signal from the low mass region prohibitively difficult. However, there may be still

hope to observe some distortions of the vector meson spectral densities. Using a dynamical simulation that accounts for a possible under-saturation of the parton chemical abundances, and estimates of the vector self-energies in a finite temperature meson gas, the yield on low invariant mass lepton pairs was calculated in Ref. [138] and is shown in Fig. 29. It can be seen

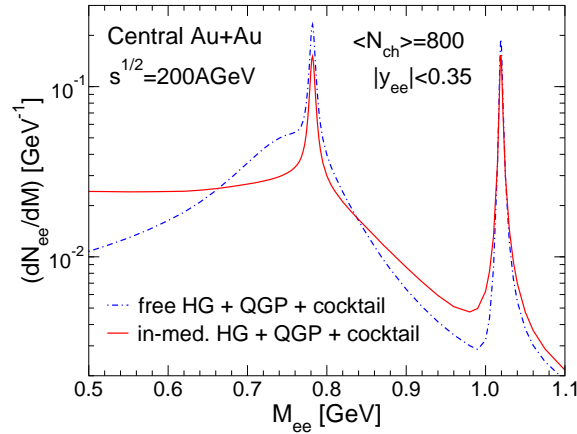


Fig. 29. Net dilepton yield from an initial plasma phase evolving into a final hadronic phase. The full and dash-dotted lines respectively represent cases with and without in-medium modifications of the vector meson spectral densities (ρ , ω , and ϕ) [138]. The “cocktail” contribution represents decays from on-shell vector mesons, at the end of the hadronic evolution.

that the in-medium effects translate into a suppression of the ρ – ω complex, and an enhancement below $M = 0.65$ GeV and above $M = 0.85$ GeV. The broadening of the ω is a candidate for experimental observation.

Moving to the intermediate mass region, one obtains¹³⁸ the results displayed in Fig. 30. In this calculation, the sensitivity of the results on parton equilibrium has been examined, and the reader is invited to consult the relevant reference for the details. The bottom line, however, is that the quark-gluon plasma contribution (as approximated by Born-term $q\bar{q}$ annihilation) does *not* dip below the Drell-Yan. This being said, the differential invariant mass distribution is predicted to be dominated by the semileptonic decays of correlated $c\bar{c}$ pairs, in the intermediate mass region¹⁴⁸. This source has

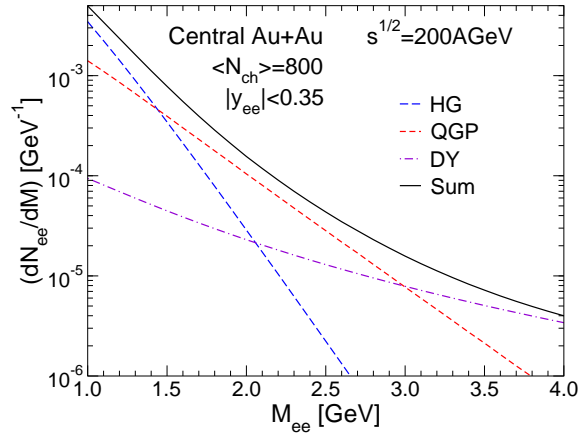


Fig. 30. Intermediate-mass lepton pair spectra at RHIC energies [138]. Contributions from the hadron gas (HG), quark-gluon plasma (QGP), and Drell-Yan (DY) are shown individually, along with their sum.

not been shown in the figures above. However, if the heavy quarks that are progenitor for the semileptonic decay lose energy in the strongly interacting medium, this background will be suppressed¹³⁹. A direct measurement would go a long way in lifting the ambiguities¹⁴⁰.

4.3. Electromagnetic Signatures of Jets

It is appropriate to discuss the electromagnetic signatures of jets in an environment devoted to predictions, as the physics necessary for those to exist necessitates high energy and intensity machines such as RHIC and the LHC. The fate of high energy jets traversing hot and dense matter is a fascinating study, and this whole subfield has become known as that of “jet quenching”. The manner in which high energy jets lose energy in a strongly interacting medium has been shown to depend on the nature of the medium itself¹⁴¹. Thus, jet tomography is expected to be a sensitive probe of the quark-gluon plasma. However, if jets and plasma interact in such a way that the jet characteristics are modified, the jet-plasma interactions could by the same token lead to the emission of electromagnetic radiation. As discussed earlier, the microscopic processes leading to real photon emission at the parton level are quark-antiquark annihilation, Compton scattering, as

well as bremsstrahlung. Therefore, a fast quark passing through the plasma will produce photons by Compton scattering with the thermal gluons and annihilation with the thermal antiquarks¹⁴². Those processes are higher-order in α_s , when compared with photons from initial hard scatterings, but they will not form a sub-leading contribution as they correspond to multiple scattering (actually, double scattering) which grows with the system size.

Working out the details, one can show that the rate of production of real photons due to annihilation and Compton scattering is¹¹⁴

$$E_\gamma \frac{dN^{(a)}}{d^4x d^3p_\gamma} = \frac{16E_\gamma}{2(2\pi)^6} \sum_{q=1}^{N_f} f_q(\mathbf{p}_\gamma) \int d^3p f_{\bar{q}}(\mathbf{p}) [1 + f_g(\mathbf{p})] \\ \times \sigma^{(a)}(s) \frac{\sqrt{s(s-4m^2)}}{2E_\gamma E} + (q \leftrightarrow \bar{q}), \quad (33)$$

$$E_\gamma \frac{dN^{(C)}}{d^4x d^3p_\gamma} = \frac{16E_\gamma}{(2\pi)^6} \sum_{q=1}^{N_f} f_q(\mathbf{p}_\gamma) \int d^3p f_g(\mathbf{p}) [1 - f_q(\mathbf{p})] \\ \times \sigma^{(C)}(s) \frac{(s-m^2)}{2EE_\gamma} + (q \rightarrow \bar{q}). \quad (34)$$

The f_i are parton distribution functions. In order to proceed one may assume that those may be decomposed as

$$f(\mathbf{p}) = f_{\text{thermal}}(\mathbf{p}) + f_{\text{jet}}(\mathbf{p}) \quad (35)$$

where the thermal component is characterised by a temperature T : $f_{\text{thermal}} = \exp(-E/T)$. This separation is kinematically reasonable as the jet spectra fall off as a power law and can thus easily be differentiated from their thermal counterpart. The phase space distribution for the quark jets propagating through the QGP is given by the perturbative QCD result for the jet yield¹⁴³:

$$f_{\text{jet}}(\mathbf{p}) = \frac{1}{g_q} \frac{(2\pi)^3}{\pi R_\perp^2 \tau p_\perp} \frac{dN_{\text{jet}}}{d^2p_\perp dy} R(r) \quad (36)$$

$$\times \delta(\eta - y) \Theta(\tau - \tau_i) \Theta(\tau_{\text{max}} - \tau) \Theta(R_\perp - r), \quad (37)$$

where $g_q = 2 \times 3$ is the spin and colour degeneracy of the quarks, R_\perp is the transverse dimension of the system, $\tau_i \sim 1/p_\perp$ is the formation time for the jet and η is the space-time rapidity. $R(r)$ is a transverse profile function. τ_{max} is the smaller of the life-time τ_f of the QGP and the time τ_d taken by the jet produced at position \mathbf{r} to reach the surface of the plasma. The boost invariant correlation between the rapidity y and η is assumed⁵⁸.

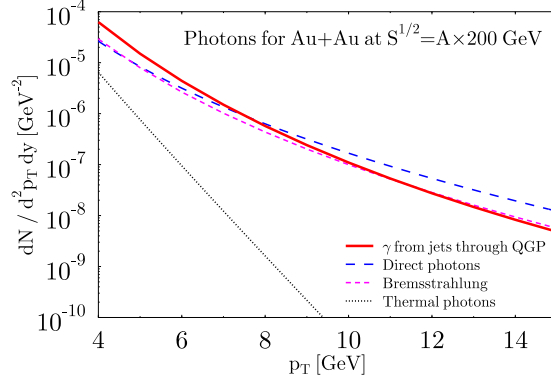


Fig. 31. Spectrum $dN/d^2p_\perp dy$ of photons at $y = 0$ for central collision of gold nuclei at $\sqrt{S_{NN}} = 200$ GeV at RHIC. Plotted¹⁴² is the yield for photons from jets interacting with the medium (solid line), direct hard photons (long dashed), bremsstrahlung photons (short dashed) and thermal photons (dotted).

Fig. 31 contains the results for thermal photons, direct photons due to primary processes, bremsstrahlung photons and the photons coming from jets passing through the QGP in central collision of gold nuclei at RHIC energies. The corresponding results for LHC energies are shown in Fig. 32. It is seen that the quark jets passing through the QGP give rise to a large yield of high energy photons. This contribution should be absent in pp collisions. For RHIC this contribution is the dominant source of photons up to $p_\perp \approx 6$ GeV. The jet-to-photon conversion falls more rapidly with p_\perp than the direct photon yield, similar to a higher twist correction. It is clear that this new mechanism for the production of high energy photons contributes significantly. In fact, it is the leading source of directly produced photons at RHIC in the region $p_T \leq 6$ GeV/ c .

Very similar considerations should apply to the production of lepton pairs, even though the details will of course change. Phase space now allows the direct annihilation of a quark and an antiquark into a dilepton. The cross section for this process is

$$\sigma(M^2) = \frac{4\pi}{3} \frac{\alpha^2}{M^2} N_c (2s+1)^2 \sum_f e_f^2, \quad (38)$$

where the sum runs over the flavour of quarks, $N_c = 3$, and s and e_f stand for the spin and the charge of the quark. Using kinetic theory, the reaction

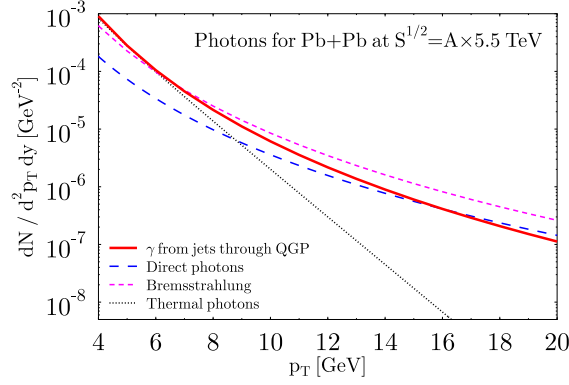


Fig. 32. The same as Fig. 31 for central collision of lead nuclei at $\sqrt{S_{NN}} = 5.5$ TeV at LHC. Taken from the same reference.

rate for the above process can be written as

$$R = \int \frac{d^3p_a}{(2\pi)^3} f_a(\mathbf{p}_a) \int \frac{d^3p_b}{2\pi^3} f_b(\mathbf{p}_b) \sigma(M^2) v_{\text{rel}}, \quad (39)$$

where f_i stands for the phase-space distribution of the quark or the anti-quark, \mathbf{p}_a and \mathbf{p}_b are their momenta respectively and the relative velocity is (for massless quarks)

$$v_{\text{rel}} = \frac{E_a E_b - \mathbf{p}_a \cdot \mathbf{p}_b}{E_a E_b}. \quad (40)$$

After some algebra this can be rewritten as

$$\begin{aligned} \frac{dR}{dM^2} &= \frac{M^6}{2} \frac{\sigma(M^2)}{(2\pi)^6} \int \tilde{x}_a d\tilde{x}_a d\phi_a \tilde{x}_b d\tilde{x}_b d\phi_b dy_a dy_b f_a f_b \\ &\times \delta [M^2 - 2M^2 \tilde{x}_a \tilde{x}_b \cosh(y_a - y_b) + 2M^2 \tilde{x}_a \tilde{x}_b \cos \phi_b] \end{aligned} \quad (41)$$

where $\tilde{x}_a = p_T^a/M$, $\tilde{x}_b = p_T^b/M$ and y_a and y_b are the rapidities. The integrations over the azimuthal angles yield

$$\begin{aligned} \frac{dR}{dM^2} &= \frac{M^4 \sigma(M^2)}{(2\pi)^5} \int \tilde{x}_a d\tilde{x}_a \tilde{x}_b d\tilde{x}_b dy_a dy_b f_a f_b \\ &\times \left[4\tilde{x}_a^2 \tilde{x}_b^2 - \{2\tilde{x}_a \tilde{x}_b \cosh(y_a - y_b) - 1\}^2 \right]^{-1/2}, \end{aligned} \quad (42)$$

such that

$$-1 \leq \frac{2\tilde{x}_a \tilde{x}_b \cosh(y_a - y_b) - 1}{2\tilde{x}_a \tilde{x}_b} \leq 1,$$

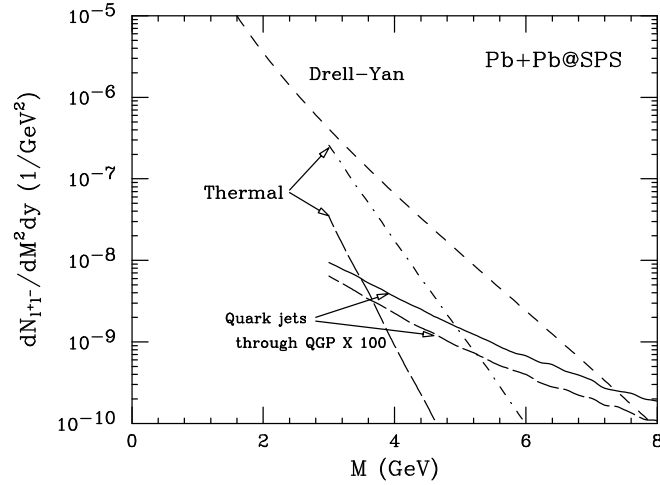


Fig. 33. Dilepton spectrum¹⁴⁴ for Pb+Pb at $\sqrt{s_{NN}} = 17.4$ GeV at SPS. The solid line is the result with $\tau_0 = 0.2$ fm/c. The long dashed curves give the results when the formation time τ_0 is raised to 0.50 fm/c, thus lowering the temperature. See the quoted reference for details.

$$\begin{aligned} 0 &\leq \tilde{x}_{a,b} \leq \infty, \\ -\infty &\leq y_{a,b} \leq \infty. \end{aligned} \quad (43)$$

When f_a and f_b are given by a thermal distribution

$$f_{\text{th}}(\mathbf{p}) = \exp(-E/T) = \exp(-p_T \cosh y/T), \quad (44)$$

the above integral can be performed to obtain Eq. (31).

Again assuming a Bjorken-scenario isentropic plasma evolution, one can plot results for thermal dileptons, dileptons from the Drell-Yan process, and the dileptons from the passage of quark jets through the plasma for SPS, RHIC, and LHC respectively. Those constitute figures 33, 34 and 35.

At SPS energies, we recover (Fig. 33) the well known result that the high mass dileptons have their origin predominantly in the Drell-Yan process. Increasing the formation time from 0.20 fm/c to 0.50 fm/c — and thus lowering the initial temperature by 100 MeV — drastically alters the thermal production (from the dash-dotted curve to the long-dashed one) while the yield from the proposed jet-plasma interaction, even though essentially negligible, is reduced by a factor of ≈ 2 (from the solid line to the long-dashed one).

The jet-plasma interaction starts playing an interesting role at RHIC

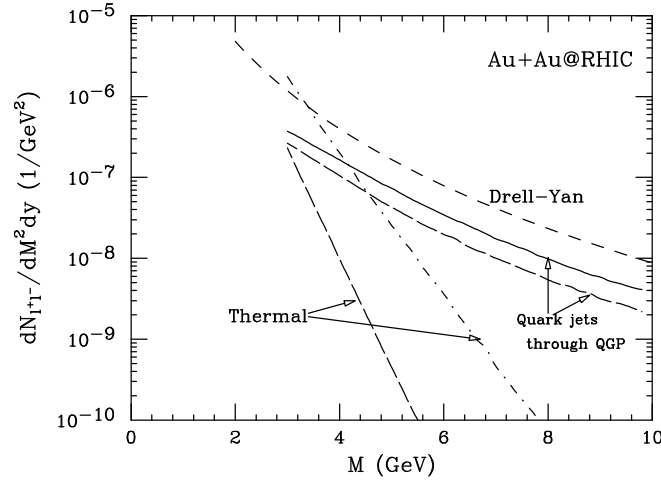


Fig. 34. Same as Fig. 33 for central Au+Au at $\sqrt{s_{NN}} = 200$ GeV at RHIC.

energies (Fig. 34), as now the corresponding yield is about only one third of the Drell-Yan contribution, and is much larger than the thermal contribution. Again lowering the initial temperature (now by about 150 MeV) by increasing the formation time to 0.50 fm/c further enhances the importance of the yield due to jet-plasma interaction. This production is of the same order as that attributed to secondary-secondary quark-antiquark annihilation in a dilepton production calculation done using an earlier version of the parton cascade model¹⁴⁵.

The much higher initial temperatures likely to be attained at the LHC and the much larger (mini)jet production lead to an excess of high mass dileptons from jet-plasma interactions which can be an order of magnitude greater (at $M = 10$ GeV) than that due to the Drell-Yan process. Again, reducing the initial temperature by raising the formation time to 0.50 fm/c reduces the jet-plasma yield by about a factor of 2 while the thermal yield is reduced far more. Recall that at LHC energies several calculations^{146,147,148} have reported a thermal yield larger than the Drell-Yan production. It is found that the jet-plasma interaction enhances the high mass dilepton production considerably. The calculations outlined above can be repeated for a plasma that is not in chemical equilibrium¹⁴⁴. In this case, conclusions similar to the ones reached above are obtained. Summarising, it appears that a unique source of high mass dileptons is

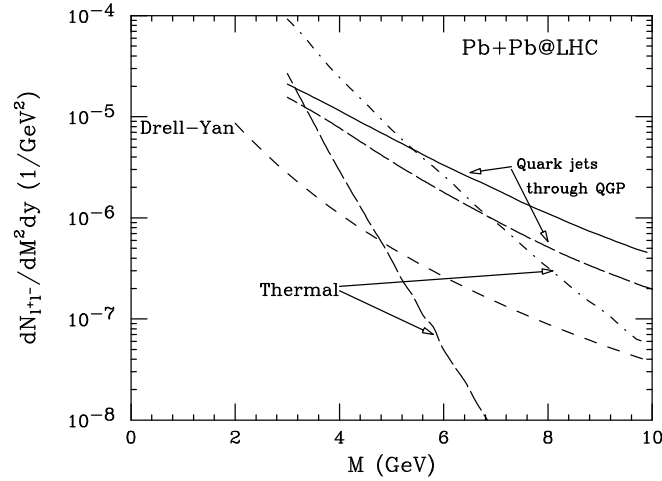


Fig. 35. Same as Fig. 33 for central Pb+Pb at $\sqrt{s_{NN}} = 5.5$ TeV at LHC.

generated by the passage of quark jets through the quark-gluon plasma. The contribution is seen to be the largest at LHC energies, moderate at RHIC energies, and negligible at SPS energies. The measurement of this radiation could then be added to the list of QGP signatures, as well as providing a proof of existence for the conditions suitable for jet-quenching to occur.

Finally, even though this is not a “direct” plasma signal, it is worth mentioning that electromagnetic radiation can also serve as a versatile jet-tag. This is especially useful in environments where the jet is expected to lose energy, or to be quenched out of existence. This statement holds true for real photons¹⁴⁹, as well as for lepton pairs¹⁵⁰.

4.4. Squeezing Lepton Pairs out of Broken Symmetries

We have seen in the text above that the electromagnetic radiation measured in nuclear collisions is a precious measure of the in-medium photon self-energy. However, in a bath of finite temperature and density, new possibilities can manifest themselves. In some sense, the medium allows for the existence of correlators that vanish identically in the vacuum. This fact opens mixing channels that were previously closed. While several studies have sought to investigate the in-medium properties of hadrons, their mixing with other hadrons has up to now received little attention. An exception

is the case of $\rho - \omega$ ¹³⁰. This specific mixing may be omitted when dealing with isospin symmetric nuclear matter, as is done here. Also, one will concentrate on vector mesons, as they enjoy a privileged relationship with electromagnetic signals. First, one describes an exploratory calculation designed to highlight an eventual signal. The possibility of $\rho - a_0$ mixing is explored, via nucleon-nucleon excitations in strongly interacting systems. It is shown that this mixing opens up a new channel for the dilepton production and may thus induce an additional peak in the ϕ region. A similar mixing exists with the $\sigma - \omega$ ^{133,134}, but its electromagnetic signatures are much smaller^{135,136}.

For the purposes described above, the interaction Lagrangian can be written as

$$\begin{aligned} \mathcal{L} = & g_\sigma \bar{\Psi} \phi_\sigma \Psi + g_{a_0} \bar{\Psi} \phi_{a_0, b} \tau^b \Psi + g_{\omega NN} \bar{\Psi} \gamma_\mu \Psi \omega^\mu \\ & + g_\rho \left[\bar{\Psi} \gamma_\mu \tau^\alpha \Psi + \frac{\kappa_\rho}{2m_N} \bar{\Psi} \sigma_{\mu\nu} \tau^\alpha \Psi \partial^\nu \right] \rho_\alpha^\mu, \end{aligned} \quad (45)$$

where Ψ , ϕ_σ , ϕ_{a_0} , ρ , and ω correspond to nucleon, σ , a_0 , ρ , and ω fields, and τ_b is a Pauli matrix. The values for the coupling parameters are from [131]. The existence of a preferred rest frame essentially creates a new vacuum state with quantum numbers different from those of the true vacuum. An immediate consequence of this fact is that one can now define a mixed correlator involving scalar and vector current operators: $\langle j^S j_\mu^V \rangle$. This mixed correlator is identically zero in the true vacuum. The polarisation vector through which the a_0 couples to the ρ via the $N - N$ loop is given by

$$\Pi_\mu(q_0, |\vec{q}|) = 2ig_{a_0}g_\rho \int \frac{d^4k}{(2\pi)^4} \text{Tr} [G(k)\Gamma_\mu G(k+q)] , \quad (46)$$

where 2 is an isospin factor and the vertex for $\rho - N - N$ coupling is

$$\Gamma_\mu = \gamma_\mu - \frac{\kappa_\rho}{2m_N} \sigma_{\mu\nu} q^\nu . \quad (47)$$

In the above $G(k)$ is the in-medium nucleon propagator¹³². For the sake of simplicity, one first uses the density-dependent and temperature-independent propagator. This approximation will be relaxed later. With the evaluation of the trace and after a little algebra, Eq. 46 can be cast in a suggestive form:

$$\Pi_\mu(q_0, |\vec{q}|) = \frac{g_{a_0}g_\rho}{\pi^3} 2q^2 \left(2m_N^* - \frac{\kappa q^2}{2m_N} \right) \int_0^{k_F} \frac{d^3k}{E^*(k)} \frac{k_\mu - \frac{q_\mu}{q^2} (k \cdot q)}{q^4 - 4(k \cdot q)^2} . \quad (48)$$

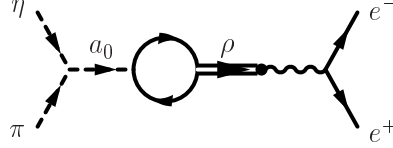


Fig. 36. Feynman diagram for the process $\pi + \eta \rightarrow e^+ e^-$, which proceeds through $\rho - a_0$ mixing.

This leads immediately to two conclusions. First, $q_\mu \Pi^\mu = 0$. Second, only two components of the polarisation vector survive after the angular integration. This will guarantee that only the longitudinal component of the ρ couples to the scalar meson, while the transverse mode remains unaltered. Further note that current conservation implies that out of the two nonzero components of Π_μ , only one is independent. The new mixing channel will affect the properties of the mesons in medium, *i.e.* affect their masses and spectral function. Those aspects will not be discussed at length here, but details can be found in the literature^{134,137}.

The $\rho - a_0$ mixing opens a new channel in dense nuclear matter, $\pi + \eta \rightarrow e^+ e^-$, which may proceed through $N-N$ excitations. The Feynman diagram for this process is shown in Fig. 36. One may then evaluate cross sections for the production of lepton pairs. Evaluating the polarisation in the zero-temperature limit, the cross section for this process is

$$\sigma_{\pi\eta \rightarrow e^+ e^-} = \frac{4\pi\alpha^2}{3q_z^2 M} \frac{g_{a_0\pi\eta}^2}{g_\rho^2} \frac{m_\rho^4}{(M^2 - m_\rho^2)^2 + m_\rho^2 \Gamma_\rho^2(M)} \times \frac{1}{(M^2 - m_{a_0})^2 + m_{a_0}^2 \Gamma_{a_0}^2(M)} \frac{1}{\sqrt{M^2 - 4m_\pi^2}} |\Pi_0|^2, \quad (49)$$

where Π_0 is the zeroth component of the expression in Eq. (46). The numerical values for the couplings and the calculation details are to be found in Ref. [151]. The cross sections are shown in Fig. 37, for two different values of the nuclear density. The familiar process $\pi\pi \rightarrow e^+ e^-$ is also plotted to set a scale. A noticeable feature of this plot is that the mixing process induces a peak at $m_{a_0} = 0.985$ GeV. This constitutes a genuine in-medium effect which is mostly density-driven: this peak would be completely absent in vacuum. Furthermore, the contribution to the cross section at the a_0 mass is comparable in magnitude to that of the $\pi\pi$ channel at its peak. Calculations of emission rates where the $T = 0$ simplification was not made also support this claim¹³⁶. Those mixing effects will also affect the bulk

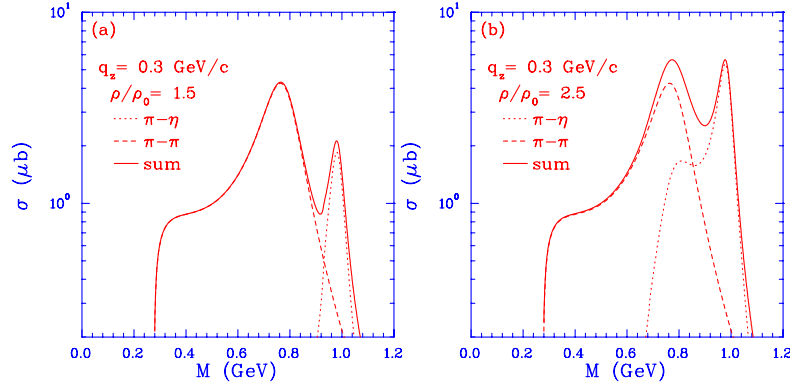


Fig. 37. Dilepton spectrum induced by $\pi + \pi \rightarrow e^+ + e^-$ and $\pi + \eta \rightarrow e^+ + e^-$ considering matter-induced $\rho - a_0$ mixing. (a) $\rho = 1.5\rho_0$ (b) $\rho = 2.5\rho_0$

features of in-medium mesonic behaviour¹³⁷. A natural question to ask is whether those symmetry-breaking effects in the dilepton spectrum should have been observed in any of the past or present experiments. It turns out that the required baryonic density is too transient to influence significantly this signal at CERN energies¹⁵². However, the HADES¹⁵³ experiment at the GSI, in Darmstadt, Germany, has the resolution and the sensitivity to explore the appropriate invariant mass range. Those heavy ion reactions are performed at lower energies, with respect to those of CERN, and thus lead to higher baryonic densities which persist longer. Evidencing continued theoretical interest at these lower energies, there are new advancements^{154,156} in theory pertinent for the dilepton measurements made by the DLS¹⁵⁵, and to be made by HADES.

There is finally another symmetry-breaking with an electromagnetic signature that will be mentioned, even though quantitative evaluations are still in their preliminary stage. At zero temperature, and at finite temperature and zero charge density, diagrams in QED that contain a fermion loop with an odd number of photon vertices are cancelled by an equal and opposite contribution coming from the same diagram with fermion lines running in the opposite direction, this is the basic content of Furry's theorem¹⁵⁷ (see also [158, 159]).

In the language of operators we note that these diagrams are encountered in the perturbative evaluation of Green's functions with an odd num-

ber of gauge field operators:

$$\langle 0 | A_{\mu_1} A_{\mu_2} \dots A_{\mu_{2n+1}} | 0 \rangle.$$

In QED we know that $CA_\mu C^{-1} = -A_\mu$, where C is the charge conjugation operator. In the case of the vacuum $|0\rangle$, we note that $C|0\rangle = |0\rangle$, as the vacuum is uncharged. As a result

$$\begin{aligned} \langle 0 | A_{\mu_1} A_{\mu_2} \dots A_{\mu_{2n+1}} | 0 \rangle &= \langle 0 | C^{-1} C A_{\mu_1} C^{-1} C A_{\mu_2} \dots A_{\mu_{2n+1}} C^{-1} C | 0 \rangle \\ &= \langle 0 | A_{\mu_1} A_{\mu_2} \dots A_{\mu_{2n+1}} | 0 \rangle (-1)^{2n+1} \\ &= -\langle 0 | A_{\mu_1} A_{\mu_2} \dots A_{\mu_{2n+1}} | 0 \rangle = 0. \end{aligned} \quad (50)$$

In an equilibrated medium at a temperature T , we not only have the expectation of the operator on the ground state but on all possible matter states weighted by a Boltzmann factor:

$$\sum_n \langle n | A_{\mu_1} A_{\mu_2} \dots A_{\mu_{2n+1}} | n \rangle e^{-\beta(E_n - \mu Q_n)},$$

where $\beta = 1/T$ and μ is a chemical potential. We are thus calculating the expectation in the grand canonical ensemble. Here, $C|n\rangle = e^{i\phi}|-n\rangle$, where $|-n\rangle$ is a state in the ensemble with the same number of antiparticles as there are particles in $|n\rangle$ and vice-versa. If $\mu = 0$ i.e., the ensemble average displays zero density then inserting the operator $C^{-1}C$ as before, we get

$$\begin{aligned} \langle n | A_{\mu_1} A_{\mu_2} \dots A_{\mu_{2n+1}} | n \rangle e^{-\beta E_n} \\ = -\langle -n | A_{\mu_1} A_{\mu_2} \dots A_{\mu_{2n+1}} | -n \rangle e^{-\beta E_n} \end{aligned} \quad (51)$$

The sum over all states will contain the mirror term $\langle -n | A_{\mu_1} A_{\mu_2} \dots A_{\mu_{2n+1}} | -n \rangle e^{-\beta E_n}$, with the same thermal weight, hence

$$\sum_n \langle n | A_{\mu_1} A_{\mu_2} \dots A_{\mu_{2n+1}} | n \rangle e^{-\beta E_n} = 0, \quad (52)$$

(the expectation over states which are excitations of the vacuum $|0\rangle$ will again be zero as in Eq. 50) and Furry's theorem still holds. However, if $\mu \neq 0$ (\Rightarrow unequal number of particles and antiparticles) then

$$\begin{aligned} \langle n | A_{\mu_1} A_{\mu_2} \dots A_{\mu_{2n+1}} | n \rangle e^{-\beta(E_n - \mu Q_n)} \\ = -\langle -n | A_{\mu_1} A_{\mu_2} \dots A_{\mu_{2n+1}} | -n \rangle e^{-\beta(E_n - \mu Q_n)}, \end{aligned} \quad (53)$$

the mirror term this time is $\langle -n | A_{\mu_1} A_{\mu_2} \dots A_{\mu_{2n+1}} | -n \rangle e^{-\beta(E_n + \mu Q_n)}$, with a different thermal weight, thus

$$\sum_n \langle n | A_{\mu_1} A_{\mu_2} \dots A_{\mu_{2n+1}} | n \rangle e^{-\beta(E_n - \mu Q_n)} \neq 0. \quad (54)$$

The sum over all medium states which leads to the expectation value is no longer zero. This represents the breaking of Furry's theorem by the medium. Note that this occurs only in media with non-zero density or chemical potential. Summarising, if the medium contains a net charge, such that it breaks C spontaneously, Green's functions that vanish identically in the vacuum (or in a neutral medium) can survive. Making the simplest possible extension to QCD, one may replace two of the photons with gluons. This enables processes like $gg \rightarrow \ell^+ \ell^-$, where the gluon fusion proceeds through a quark (antiquark) loop. This channel is exciting for the following reason: it offers a direct electromagnetic signature of early gluon populations. This represents pristine information on the state of the many-body system. Calculations are technically involved¹⁶⁰, but results are finally forthcoming¹⁶¹.

5. Conclusions

This ends our survey of the use of electromagnetic signals as probes of strongly-interacting relativistic many-body dynamics. The supporting framework has been relativistic quantum field theory, generalised to finite temperatures and densities, in order to formulate very general computational tools for estimating production rates from heated and compressed nuclear systems. The focus was on establishing within equilibrium circumstances, the number of radiated electromagnetic quanta per unit volume per unit time. For then, one can, and did, take the rate and evolve according to some "best guess" scenarios for the expansion dynamics in heavy ion collisions realized at facilities at SPS and RHIC.

Dilepton experimental circumstances resembling those expected at the CERN SPS have been modeled in a variety of ways. Comparisons of theory and experiment have been fruitful in terms of suggesting a consistent picture of modified vector meson spectral properties. These modifications are truly collective nuclear effects. Tremendous advancement in our understanding of the way in which nuclear matter responds when it is forced near the phase boundary between hadrons and quarks has come from these pursuits. To mention some specific achievements, one notes that the rho spectral

function has been essentially measured at finite energy density and has been shown to be significantly modified from its vacuum structure. This is a significant achievement.

The photon studies have been exceptionally fruitful too. Theory has advanced from a stage where rate estimates were plagued with infrared singularities, to first establishing regulated lowest-order results with new computational techniques and tools. The hard-thermal-loop approach is useful not only for photon production, but other studies in hot gauge theories and for a variety of observables. Next, one witnessed an impressive effort to understand the photon self-energy up to the many-loop order and including multiple-scattering effects within the medium. The celebrated result is a complete lowest order photon production rate from finite temperature QCD that is stable and reliable. That too is a nontrivial accomplishment.

When the QCD rates and hadronic rates are used to predict photon yields and then compared with experiments WA80 and WA98 from CERN, there is consistency, if not discriminatory features. One can say that the results strongly suggest thermal emission from a fireball at roughly 200 MeV temperature. Have we observed the QGP? The investigations reported on in this work only contain hints of an answer. As mentioned previously, the radiation from the partonic phase is present in the analyses, but does not constitute a large portion of the overall signal. Fortunately, this state of affairs is directly related to probed temperatures and to the space-time volume occupied by the plasma. Both those are expected to increase in the current and future generations of collider experiments. The only indirect proof is that, in many dynamical simulations, it is unavoidable for the initial phase to be elsewhere in the phase diagram than in the deconfined region. This is a consistency requirement brought about by our current knowledge of the equation of state. This however will change and evolve, especially with the experience gained with non-perturbative approaches which will in turn guarantee a better focused picture of the quasiparticle nature of the partonic sector. Have we observed chiral symmetry restoration? The approach to chiral symmetry is closely related to the properties of the in-medium spectral densities¹⁶². As the constraints of the Weinberg sum rules are extended to finite temperatures, they require a degeneracy of the vector and axial-vector correlators in the symmetric limit. This demand, however, can be satisfied in several ways¹⁶². Thus, a verdict on the status of chiral symmetry restoration is being hindered by the difficulty to access the axial-vector correlator unambiguously. More theoretical work needs to be done in that respect as well, in order to provide a unified calculation with a credible

degree of sophistication. It should finally be mentioned that RHIC and the LHC will have the intensity to make possible Hanbury-Brown-Twiss interferometry measurements of direct photons. The theory of this observable is well-developed¹⁶³, and measurements of the correlation functions are expected to place constraints on the space-time extent of the photon-emitting sources¹⁶⁴.

If the estimates brought about by dynamical approaches and by analyses of hadrons abundances are reliable, we have just grazed the phase boundary of the deconfined sector at the SPS. This assertion is not in conflict with the evidence obtained from measurements of electromagnetic observables. Then, RHIC, and the LHC, should soon signal bold incursions into a new territory.

Acknowledgements

It is a pleasure to acknowledge helpful comments from, and discussions with, P. Aurenche, J.-e. Alam, A. Bourque, E. Bratkovskaya, A. Dutt-Mazumder, S. Gao, F. Gélis, P. Jaikumar, B. Kämpfer, J. Kapusta, V. Koch, I. Kvasnikova, G. D. Moore, R. Rapp, D. Srivastava, O. Teodorescu, Y. Tserruya, and S. Turbide. C. G. thanks J. Bruce, J. Entwistle, J. Pastorius, Ch. Squire, and G. Willis for inspiration. This work has been supported in part by the Natural Sciences and Engineering Research Council of Canada, in part by the the Fonds Nature et Technologies of Quebec, and in part by the National Science Foundation under grant number PHY-0098760.

References

1. F. Karsch and E. Laermann, this volume; F. Karsch, AIP Conf. Proc. **631**, 112 (2003).
2. K. Kanaya, Nucl. Phys. A **715**, 233c (2003).
3. Z. Fodor and F. Karsch, JHEP **03**, 014 (2002).
4. M. Stephanov, K. Rajagopal, and E. Shuryak, Phys. Rev. Lett. **81**, 4816 (1998).
5. See, for example, K. Rajagopal and F. Wilczek, *At the Frontiers of Particle Physics/Handbook of QCD*, M. Shifman ed., (World Scientific, Singapore, 2000), and references therein.
6. Prashanth Jaikumar, Ralf Rapp, and Ismail Zahed, Phys. Rev. C **65**, 055205 (2002).
7. E. L. Feinberg, Nuovo Cimento **34A**, 391 (1976).
8. L.D. McLerran and T. Toimela, Phys. Rev. D **31**, 545 (1985).
9. C. M. Ko, L. H. Xia, and P. J. Siemens, Phys. Lett. **B231**, 16 (1989).
10. H. A. Weldon, Phys. Rev. D **42**, 2384 (1990).

11. C. Gale and J. I. Kapusta, Nucl. Phys. **B357**, 65 (1991).
12. E. S. Fradkin, Proc. Lebedev Physics Institute **29**, 6 (1965).
13. See, for example, Michael E. Peskin and Daniel V. Schroeder, *An Introduction to Quantum Field Theory*, (Addison-Wesley, Reading, 1995), and references therein.
14. Charles Gale and Peter Lichard, Phys. Rev. C **49**, 3338 (1994).
15. G. Chanfray and P. Schuck, Nucl. Phys. **A555**, 329 (1993).
16. G. Chanfray, R. Rapp, and J. Wambach, Phys. Rev. Lett. **76**, 368 (1996).
17. R. Rapp, G. Chanfray, and J. Wambach, Nucl. Phys. **A617**, 472 (1997).
18. J. J. Sakurai, *Currents and Mesons*, (University of Chicago Press, Chicago, 1969).
19. F. Klingl, N. Kaiser, and W. Weise, Z. Phys. A **356**, 193 (1996).
20. H. B. O'Connell, B. C. Pearce, A. W. Thomas, and A. G. Williams, Prog. Part. Nucl. Phys. **39**, 201 (1997).
21. Ralf Rapp and Charles Gale, Phys. Rev. C **60**, 024903 (1999).
22. Sangyong Jeon and Paul. J. Ellis, Phys. Rev. D **58**, 045013 (1998).
23. W. Cassing and E. L. Bratkovskaya, Phys. Rept. **308**, 65 (1999).
24. R. Rapp and J. Wambach, Adv. Nucl. Phys. **25**, 1 (2000).
25. P. Huovinen, M. Belkacem, P.J. Ellis, and J.I. Kapusta, Phys. Rev. C **66**, 014903 (2002).
26. G. Agakichiev *et al.*, Phys. Rev. Lett. **75**, 1272 (1995); Phys. Lett. **B422**, 405 (1998).
27. M. Masea *et al.*, Nucl. Phys. **A590**, 93c (1995).
28. G. E. Brown and Mannque Rho, Phys. Rept. **269**, 333 (1996).
29. See, for example, C. Gale, Nucl. Phys. **A698**, 143 (2002), and references therein.
30. Johannes P. Wessels *et al.* (CERES collaboration), Nucl. Phys. **A715**, 262c (2003).
31. E. Shuryak, Phys. Lett. **B79**, 135 (1978).
32. A. L. S. Angelis *et al.*, Eur. Phys. J. C **13**, 433 (2000).
33. M. C. Abreu *et al.*, Phys. Lett. **B368**, 230 (1996); Nucl. Phys. **A610**, 331 (1996).
34. C. Y. Wong and Z. Q. Wang, Phys. Lett. **B367**, 50 (1996).
35. C. Spieles *et al.*, Eur. Phys. J. C **5**, 349 (1998).
36. Z. Lin and X. N. Wang, Phys. Lett. **B444**, 245 (1998).
37. L. Capelli, PhD thesis, Université Claude Bernard, 2001.
38. P. Levai, B. Müller, and X. N. Wang, Phys. Rev. C **51**, 3326 (1995).
39. P. Bordalo *et al.*, Nucl. Phys. **A661**, 538c (1999).
40. G. Q. Li and C. Gale, Phys. Rev. Lett. **81**, 1572 (1998); Phys. Rev. C **58**, 2914 (1998).
41. L. Xiong, E. V. Shuryak, and G. E. Brown, Phys. Rev. D **46**, 3798 (1992); C. Song, C. M. Ko, and C. Gale, Phys. Rev. D **50**, R1827 (1994); J. K. Kim *et al.*, Phys. Rev. D **53**, 4787 (1996).
42. Particle Data Group, Phys. Rev. D **66**, 010001 (2002).
43. S. Gao and C. Gale, Phys. Rev. C **57**, 254 (1998).
44. L. M. Barkov *al.*, (OLYA collaboration), Nucl. Phys. **B256**, 365 (1985).

45. D. Bisello *et al.*, (DM2 collaboration), Phys. Lett. **B220**, 321 (1989).
46. M. E. Biagini, S. Dubnicka, E. Etim, and P. Kolar, Nuovo Cimento A **104**, 363 (1991).
47. R. R. Akhmetshin *et al.*, (CMD-2 collaboration), Phys. Lett. **B364**, 199 (1995).
48. D. Bisello *et al.*, (DM2 collaboration), Z. Phys. C **39**, 13 (1988).
49. P. M. Ivanov *et al.*, (OLYA collaboration), Phys. Lett. **B107**, 297 (1981).
50. K. Haglin and C. Gale, Phys. Rev. D **52**, 6297 (1995).
51. S. I. Dolinsky *et al.*, (ND collaboration), Phys. Rept. **202**, 99 (1991).
52. N. Albrecht *et al.*, (ARGUS collaboration), Phys. Lett. **B185**, 223 (1987).
53. H. Gomm, Ö. Kaymakçalan, and J. Schechter, Phys. Rev. D **30**, 2345 (1984).
54. D. Bisello *et al.*, (DM2 Collaboration), Proceedings of Hadrons '91, (College Park, 1991).
55. Z. Huang, Phys. Lett. **B361**, 131 (1995).
56. I. Kvasnikova, PhD thesis, McGill University, 2001.
57. Z. Huang, private communication.
58. J. D. Bjorken, Phys. Rev. D **27**, 140 (1983); R. C. Hwa and K. Kajantie, *ibid.* **32**, 1109 (1985); M. Gyulassy and T. Matsui, Phys. Rev. D **29**, 419 (1984).
59. J. Cleymans, K. Redlich, and D. K. Srivastava, Phys. Rev. C **55**, 1431 (1997); Phys. Lett. **B420**, 261 (1998).
60. Ioulia Kvasnikova, Charles Gale, and Dinesh Srivastava, Phys. Rev. C **65**, 064903 (2002).
61. K. Gallmeister, B. Kämpfer, O.P. Pavlenko, and C. Gale, Nucl. Phys. **A688**, 939 (2001).
62. R. Rapp and E. Shuryak, Phys. Lett. **B473**, 13 (2000).
63. D. K. Srivastava, B. Sinha, I. Kvasnikova, and C. Gale, Nucl. Phys. **A698**, 432c (2002).
64. M. C. Abreu *et al.* (NA50 Collaboration), Eur. Phys. J. C **14**, 443 (2000).
65. D. K. Srivastava, Phys. Rev. C **64**, 064901 (2001); J.-Y. Ollitrault, Phys. Lett. **B273**, 31 (1991).
66. J.I. Kapusta, P. Lichard, and D. Seibert, Phys. Rev. D **44** 2774 (1991); Erratum-*ibid.* **D47**, 4171 (1993).
67. P. Singer, Phys. Rev. **130** 2441 (1963); **161** 1694 (1967).
68. H. Nadeau, J.I. Kapusta, and P. Lichard, Phys. Rev. C **45**, 3034 (1992); Erratum Phys. Rev. C **47**, 2426 (1993).
69. L. Xiong, E. Shuryak and G.E. Brown, Phys. Rev. D **46** 3798 (1992).
70. C. Song, Phys. Rev. C **47** 2861 (1993).
71. Ralf Rapp, Simon Turbide, and Charles Gale, in preparation.
72. M. Halász, J.V. Steele, G. Li, G.E. Brown, Phys. Rev. C **58** 365 (1998).
73. K. Haglin, Phys. Rev. C **50** 1688 (1994).
74. K.L. Haglin, Nucl. Phys. A **584** 719 (1995).
75. G.E. Brown and M. Rho, Phys. Rev. Lett. **66** 2720 (1991).
76. S. Sarkar, J. Alam, P. Roy, A.K. Dutt-Mazumder, B. Dutta-Roy, and B. Sinha, Nucl. Phys. A **634** 206 (1998).
77. C. Song and G. Fai, Phys. Rev. C **58** 1689 (1998).
78. P. Roy, S. Sarkar, J. Alam, and B. Sinha, Nucl. Phys. A **653** 277 (1999).

79. J.V. Steele, H. Yamagishi, and I. Zahed, Phys. Lett. B **384** 255 (1996).
80. J.V. Steele, H. Yamagishi, and I. Zahed, Phys. Rev. D **56** 5605 (1997).
81. H.A. Weldon, Phys. Rev. D **28**, 2007 (1983); R. L. Kobes and G. W. Semenoff, Nucl. Phys. **B260**, 714 (1985); S. M. H. Wong, Phys. Rev. D **64**, 025007 (2001); A. Majumder and C. Gale, Phys. Rev. C **65**, 055203 (2002).
82. E.V. Shuryak, Yad. Fiz. **28**, 796 (1978).
83. K. Kajantie and H.I. Miettinen, Z. Phys. C **9**, 341 (1981).
84. R.C. Hwa and K. Kajantie, Phys. Rev. D **32**, 1109 (1985).
85. R. Baier, H. Nakkagawa, A. Niegawa, and K. Redlich, Z. Phys. C **53**, 433 (1992).
86. R.D. Pisarski, Nucl. Phys. **309**, 476 (1988); Phys. Rev. Lett. **63**, 1129 (1989).
87. E. Braaten and R.D. Pisarski, Nucl. Phys. B **337**, 569 (1990).
88. T. Peitzmann and M. Thoma, Phys. Rept. **364**, 175 (2002).
89. P. Aurenche, F. Gélis, H. Zaraket, and R. Kobes, Phys. Rev. D **58**, 085003 (1998).
90. P. Arnold, G.D. Moore, and L.G. Yaffe, JHEP **0112**, 009 (2001).
91. P. Aurenche, F. Gélis, H. Zaraket, Phys. Rev. D **61**, 116001 (2000).
92. P. Aurenche, F. Gélis, H. Zaraket, Phys. Rev. D **62**, 096012 (2000b).
93. L.D. Landau and I. Pomeranchuk, Dokl. Akad. Nauk Ser. Fiz. **92**, 535 (1953).
94. A.B. Migdal, Phys. Rev. **103**, 1811 (1956).
95. R. Albrecht et al., The WA80 Collaboration, Phys. Rev. Lett. **76**, 3506 (1996).
96. M.M. Aggarwal et al., The WA98 Collaboration, Phys. Rev. Lett. **85**, 3595 (2000).
97. E.V. Shuryak and L. Xiong, Phys. Lett. B **333**, 316 (1994); Erratum, *ibid.*, B **339**, 334 (1994).
98. D.K. Srivastava and B. Sinha, Phys. Rev. Lett., **73**, 2421 (1994).
99. A. Dumitru, U. Katscher, J.A. Maruhn, H. Stöcker, W. Greiner, and D.H. Rischke, Phys. Rev. C **51**, 2166 (1995).
100. D.K. Srivastava and B. Sinha, Eur. Phys. J. C **12** 109 (2000); Erratum, *ibid.*, C **20** 397 (2000).
101. J. Cleymans, K. Redlich, and D.K. Srivastava, Phys. Rev. C **55**, 1431 (1997).
102. C. Y. Wong and H. Wang, Phys. Rev. C **58**, 376 (1998).
103. P. Aurenche, R. Baier, M. Fontannaz, and D. Schiff, Nucl. Phys. **B286**, 509 (1987); Nucl. Phys. **B297**, 661 (1988).
104. J. C. Collins, D. E. Soper, and G. Sterman, Nucl. Phys. **B250**, 199 (1985).
105. P. Aurenche *et al.*, Eur. Phys. J. C **9**, 107 (1999).
106. Geoffrey T. Bodwin, Stanley J. Brodsky, and G. Peter Lepage, Phys. Rev. D **39**, 3287 (1989).
107. A. Dumitru, L. Frakfurt, L. Gerland, H. Stöcker, and M. Strikman, Phys. Rev. C **64**, 054909 (2001).
108. K. Gallmeister, B. Kämpfer, and O. P. Pavlenko, Phys. Rev. C **62**, 057901 (2000).
109. D.K. Srivastava and B. Sinha, Phys. Rev. C **64** 034902 (2001).
110. J.-e Alam, S. Sarkar, T. Hatsuda, T.K. Nayak, and B. Sinha, Phys. Rev. C **63**, 021901R (2001).

111. J. Sollfrank, P. Huovinen, M. Kataja, P.V. Ruuskanen, M. Prakash, and R. Venugopalan, Phys. Rev. C **55**, 392 (1997).
112. P. Huovinen, P.V. Ruuskanen, and J. Sollfrank, Nucl. Phys. A **650**, 227 (1999).
113. P. Huovinen, P. V. Ruuskanen, and S. S. Räsänen, Phys. Lett. B **535**, 109 (2002).
114. C. Y. Wong, *Introduction to Heavy Ion Collisions*, (World Scientific, Singapore, 1994).
115. Steffen A. Bass, Berndt Müller, and Dinesh K. Srivastava, Phys. Rev. Lett. **90**, 082301 (2003).
116. K. Geiger and B. Müller, Nucl. Phys. **B369**, 600 (1992).
117. S. A. Bass, B. Müller, and D. K. Srivastava, Phys. Lett. B **551**, 277 (2003).
118. E. Braaten, R.D. Pisarski, and T.C. Yuan, Phys. Rev. Lett. **64**, 2242 (1990).
119. S. M. H. Wong, Z. Phys. C **53**, 465 (1992).
120. K. Haglin, C. Gale, and V. Emel'yanov, Phys. Rev. D **47**, 973 (1993).
121. P. Aurenche, F. Gélis, and H. Zaraket, JHEP **0207** 063 (2002).
122. P. Aurenche, F. Gélis, G.D. Moore and H. Zaraket, JHEP **0212** 006 (2002).
123. T. Altherr, P.V. Ruuskanen, Nucl. Phys. **380**, 377 (1992).
124. M. H. Thoma and C.T. Traxler, Phys. Rev. D **56**, 198 (1997).
125. For a review of this technology, see M. Jarrel and J.E. Gubernatis, Phys. Rept. **269**, 133 (1996).
126. I. Wetzorke, hep-lat/0305012; M. Asakawa, T. Hatsuda, and Y. Nakahara, Nucl. Phys. A **715**, 863c (2003).
127. N. Hammon *et al.*, Phys. Rev. C **57**, 3292 (1998).
128. D.Y. Peressounko and Y.E. Pokrovsky, Nucl. Phys. A **669**, 196 (2000).
129. F.D. Steffen and M. H. Thoma, Phys. Lett. B **510**, 98 (2001).
130. A. K. Dutt-Mazumder, B. Dutta-Roy, and A. Kundu, Phys. Lett. **B399**, 196 (1997); W. Broniowski and W. Florkowski, Phys. Lett. **B440**, 7 (1998).
131. R. Machleidt, Adv. Nucl. Phys. **19**, 198 (1989).
132. B. Serot and J. D. Walecka, Adv. Nucl. Phys. **16**, 1 (1986).
133. S. A. Chin, Ann. Phys. (N.Y.), **108**, 301 (1977).
134. K. Saito, K. Tsushima, A. W. Thomas, A. G. Williams, Phys. Lett. **B433**, 243 (1998).
135. H. A. Weldon, Phys. Lett. **B274**, 133 (1992); G. Wolf, B. Friman, and M. Soyeur, Nucl. Phys. **A640**, 129 (1998).
136. O. Teodorescu, A. K. Dutt-Mazumder, and Charles Gale, Phys. Rev. C **63**, 034903 (2001).
137. O. Teodorescu, A. K. Dutt-Mazumder, and Charles Gale, Phys. Rev. C **66**, 015209 (2002).
138. Ralf Rapp, Phys. Rev. C **63**, 054907 (2001).
139. E. Shuryak, Phys. Rev. C **55**, 961 (1997); Z. Lin, R. Vogt, and X.-N. Wang, *ibid* **57**, 899 (1998); B. Kämpfer and O. P. Pavlenko, Phys. Lett. B **391**, 185 (1997).
140. <http://na60.web.cern.ch/NA60/>
141. Miklos Gyulassy, Ivan Vitev, Xin-Nian Wang, and Ben-Wei Zhang, this volume.

142. Rainer J. Fries, Berndt Müller, and Dinesh K. Srivastava, Phys. Rev. Lett. **90**, 132301 (2003).
143. Z. Lin and M. Gyulassy, Phys. Rev. C **51**, 217 (1995).
144. Dinesh K. Srivastava, Charles Gale, and Rainer J. Fries, Phys. Rev. C **67**, 034903 (2003).
145. K. Geiger and J. I. Kapusta, Phys. Rev. Lett. **70**, 1920 (1993).
146. J. Kapusta, L. D. McLerran and D. K. Srivastava, Phys. Lett. B **283**, 145 (1992).
147. D. K. Srivastava, M. G. Mustafa and B. Müller, Phys. Rev. C **56**, 1064 (1997).
148. R. Vogt, B. V. Jacak, P. L. McGaughey and P. V. Ruuskanen, Phys. Rev. D **49**, 3345 (1994); S. Gavin, P. L. McGaughey, P. V. Ruuskanen and R. Vogt, Phys. Rev. C **54**, 2606 (1996); D. Fein, Z. P. Valerio and I. Sarcevic, Phys. Rev. C **56**, 1637 (1997).
149. X. N. Wang, Z. Huang, and I. Sarcevic, Phys. Rev. Lett. **77**, 231 (1996); X. N. Wang and Z. Huang, Phys. Rev. C **55**, 3047 (1997).
150. Dinesh K. Srivastava, Charles Gale, and T. C. Awes, Phys. Rev. C, in press.
151. O. Teodorescu, A. K. Dutt-Mazumder, and C. Gale, Phys. Rev. C **61**, 051901(R) (2000).
152. O. Teodorescu, PhD thesis, McGill University 2002.
153. J. Friese *et al.*, Prog. Part. Nucl. Phys. **42**, 235 (1999).
154. E. L. Bratkovskaya, W. Cassing, M. Effenberger, and U. Mosel, Nucl. Phys. A **653**, 301 (1999); E. L. Bratkovskaya, W. Cassing, and U. Mosel, *ibid.* **686**, 568 (2001); E. L. Bratkovskaya, *ibid.* **696**, 309 (2001).
155. R. J. Porter *et al.*, Phys. Rev. Lett. **79**, 1229 (1997); W. K. Wilson *et al.*, Phys. Rev. C **57**, 1865 (1998).
156. R. Shyam and U. Mosel, hep-ph/0303035; K. Schekhter *et al.*, nucl-th/0305015.
157. W. H. Furry, Phys. Rev. **51**, 135 (1937).
158. C. Itzykson and J. B. Zuber, *Quantum Field Theory*, McGraw Hill, New York, (1980).
159. S. Weinberg, *The Quantum Theory of Fields*, Vol. 1, Cambridge University Press, (1995).
160. A. Majumder, PhD thesis, McGill University 2002; A. Bourque, MSc thesis, McGill University 2002.
161. A. Bourque, A. Majumder, and C. Gale, in preparation.
162. J. I. Kapusta and Edward V. Shuryak, Phys. Rev. D **49**, 4694 (1994).
163. R. Hanbury-Brown and R. Q. Twiss, Nature **178**, 1046 (1956); G. Goldhaber, S. Goldhaber, W. Lee, and A. Pais, Phys. Rev. **120**, 300 (1960); U. Heinz and B. Jacak, Ann. Rev. Nucl. Part. Sci. **49**, 529 (1999); R. M. Weiner, Phys. Rept. **327**, 249 (2000).
164. D. Neuhauser, Phys. Lett. B **182**, 289 (1986); D. K. Srivastava and J. I. Kapusta, Phys. Lett. B **307**, 1 (1993); D. K. Srivastava and C. Gale, Phys. Lett. B **319**, 407 (1993); D. Peressounko, Phys. Rev. C **67**, 014905 (2003); Jan-e Alam *et al.*, Phys. Rev. C **67**, 054902 (2003).